1-1-2009

A Continuum-Based Model for Analysis of Laterally Loaded Piles in Layered Soils

D Basu
University of Connecticut - Storrs

Rodrigo Salgado
Purdue University, rodrigo@ecn.purdue.edu

Monica Prezzi
Purdue University, mprezzi@purdue.edu

Basu, D., Salgado, R. & Prezzi, M. (2009). *Géotechnique* **59**, No. 2, 127–140 [**doi:** 10.1680/geot.2007.00011

A continuum-based model for analysis of laterally loaded piles in layered soils

D. BASU*, R. SALGADO† and M. PREZZI†

An analysis is developed to calculate the response of laterally loaded piles in multilayered elastic media. The displacement fields in the analysis are taken to be the products of independent functions that vary in the vertical, radial and circumferential directions. The governing differential equations for the pile deflections in different soil layers are obtained using the principle of minimum potential energy. Solutions for pile deflection are obtained analytically, whereas those for soil displacements are obtained using the one-dimensional finite difference method. The input parameters needed for the analysis are the pile geometry, the soil profile, and the elastic constants of the soil and pile. The method produces results with accuracy comparable with that of a three-dimensional finite element analysis but requires much less computation time. The analysis can be extended to account for soil non-linearity.

KEYWORDS: elasticity; piles; theoretical analysis

Dans la présente communication, on conçoit une analyse permettant de calculer la réaction de pieux à charge latérale dans des milieux élastiques multicouches. Les champs de déplacement dans cette analyse sont censés être les produits de fonctions indépendantes variant dans les sens vertical, radial et circonférentiel. Les équations différentielles déterminantes pour les flèches des pieux dans différentes couches de terrain s'obtiennent en appliquant le principe de l'énergie potentielle minimale. Les solutions s'obtiennent de différentes façons : de façon analytique pour la flèche des pieux, et avec une méthode des différences finies unidimensionnelles pour les déplacements du sol. Les paramètres d'entrée nécessaires pour l'analyse sont la géométrie des pieux, le profil du terrain, et les constantes élastiques du sol et des pieux. Cette méthode permet d'obtenir des résultats dont la précision est comparable à celle des analyses tridimensionnelles aux éléments finis, mais qui nécessite des temps de calcul beaucoup plus courts. En outre, il est possible de renforcer cette analyse pour tenir compte de la non linéarité du terrain.

INTRODUCTION

Piles subjected to lateral forces and moments at the head are analysed in practice with the p–y method (Reese & Cox, 1969; Matlock, 1970; Reese *et al.*, 1974, 1975; Reese & Van Impe, 2001). In the p–y method the pile is assumed to behave as an Euler–Bernoulli beam with the soil modelled as a series of discretely spaced springs, each connected to one of the pile segments into which the pile is discretised. The springs model the soil response to loading through p–y curves (p is the unit resistance per unit pile length offered by the springs, and y is the pile deflection), which are developed empirically by adjusting the curves until they match actual load–displacement results (Cox *et al.*, 1974; Briaud *et al.*, 1984; Yan & Byrne, 1992; Brown *et al.*, 1994; Gabr *et al.*, 1994; Briaud, 1997; Wu *et al.*, 1998; Bransby, 1999; Ashour & Norris, 2000). However, the p–y method often fails to predict pile response (Anderson *et al.*, 2003; Kim *et al.*, 2004), for it is not capable of capturing the complex three-dimensional interaction between the pile and the soil.

The continuum approach is conceptually more appealing; however, in order to model the soil as a continuum, the use of numerical techniques such as the three-dimensional (3D) finite element (FE) method, finite elements with Fourier analysis, the boundary element (BE) method or the finite difference (FD) method is often required (Poulos, 1971a, 1971b; Banerjee & Davis, 1978; Randolph, 1981; Budhu & Davies, 1988; Brown *et al.*, 1989; Verruijt & Kooijman, 1989; Trochanis *et al.*, 1991; Bransby, 1999; Ng & Zhang, 2001; Klar & Frydman, 2002). The 3D FE or FD method can capture the most important features of the complex pile–soil interaction, but three-dimensional analyses are computationally expensive for routine practice. The BE method accounts for the pile–soil interaction by discretising the pile into small strips and modelling the interaction between these strips with the soil continuum through numerical integration of Mindlin's solution (Mindlin, 1936) for a point force within a continuum.

Considering the soil surrounding the pile as a continuum, Sun (1994), Zhang *et al.* (2000) and Guo & Lee (2001) developed closed-form solutions based on linear elasticity that can be used to obtain lateral pile deflection with depth. Their analyses capture the three-dimensional aspects of the interaction of the pile–soil system and produce results quickly, which is advantageous in practice. However, these authors made an assumption that the variation of displacements within the soil mass depends on the same displacement function for both the radial and the circumferential directions. This leads to a soil response that is stiffer than it is in reality.

Most continuum analyses of laterally loaded piles do not consider soil layering. Soil heterogeneity with depth has been approximately taken into account in the BE and FE analyses by assuming (typically) a linear variation of soil modulus with depth (Poulos, 1973; Randolph, 1981; Budhu & Davies, 1988). The BE analysis has also been used to analyse two-layer systems (Banerjee & Davies, 1978; Pise, 1982). However, BE analysis of laterally loaded piles is strictly not applicable to layered systems, because Mindlin's solution used in BE analysis is valid only for homogeneous continuums. Verruijt & Kooijman (1989) solved a layered elastic system by discretising the soil layers using FE and the pile by FD methods.

In this paper, an advanced continuum-based method of analysis of laterally loaded piles is proposed by assuming the soil displacement field to have a shape that is consistent

Manuscript received 18 February 2007; revised manuscript accepted 24 September 2008. Published online ahead of print 3 December 2008.
Discussion on this paper closes on 1 August 2009, for further details see p. ii.
* Department of Civil and Environmental Engineering, University of Connecticut, Storrs, USA
† School of Civil Engineering, Purdue University, West Lafayette, USA.

with the drop in displacement expected as distance from the pile increases, and with the fact that the displacement is expected to depend on the direction of the load with respect to the point considered in the soil. The analysis considers a pile embedded in a multilayered elastic soil (continuum), and rigorously takes into account the three-dimensional pile–soil interaction. The governing differential equations for the pile and soil displacements are developed using variational principles. Closed-form solutions are obtained for pile deflection, and soil displacements are obtained using the one-dimensional (1D) FD method. Pile response obtained using this method compares favourably with 3D FE analysis, although the computation effort required by this method is small. Because soil displacements and strains can be calculated alongside pile deflection using this method, the analysis forms the basis for future analysis that can model the interaction of piles in a group, and can account for soil nonlinearity by relating the progressive degradation of soil stiffness to induced soil strains.

ANALYSIS

Problem definition

We consider a pile with a circular cross-section of radius r_p and length L_p embedded in a soil deposit that has n layers (Fig. 1). Each layer extends to infinity in all radial directions, and the bottom (nth) layer extends to infinity in the downward direction. The vertical depth to the base of any intermediate layer i is H_i, which implies that the thickness of the ith layer is $H_i - H_{i-1}$ with $H_0 = 0$ and $H_n = \infty$. The pile head is at the ground surface, and the base is embedded in the nth layer. The pile is subjected to a horizontal force F_a and a moment M_a at the pile head such that F_a and M_a are orthogonal vectors. In the analysis, we choose a cylindrical (r–θ–z) coordinate system with its origin coinciding with the centre of the pile head and the positive z-axis (coinciding with the pile axis) pointing downwards. The goal of the analysis is to obtain pile deflection as a function of depth caused by the action of F_a and/or M_a at the pile head.

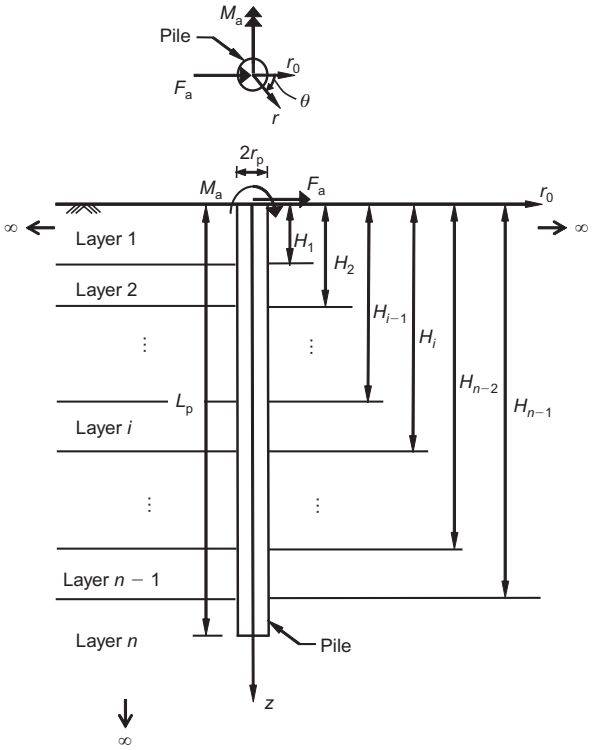

Fig. 1. Laterally loaded pile in layered elastic medium

The soil medium is assumed to be an elastic and isotropic continuum, homogeneous within each layer, with Lame's constants λ_s and G_s. There is no slippage or separation between the pile and the surrounding soil, or between the soil layers. The pile behaves as an Euler–Bernoulli beam with a constant flexural rigidity E_pI_p.

Potential energy

The total potential energy of the pile–soil system, including both the internal and external potential energies, is given by

$$\Pi = \frac{1}{2}E_pI_p\int_0^{L_p}\left(\frac{d^2w}{dz^2}\right)^2 dz + \int_0^{\infty}\int_0^{2\pi}\int_{r_p}^{\infty}\frac{1}{2}\sigma_{pq}\varepsilon_{pq}r\,dr\,d\theta\,dz + \int_{L_p}^{\infty}\int_0^{2\pi}\int_0^{r_p}\frac{1}{2}\sigma_{pq}\varepsilon_{pq}r\,dr\,d\theta\,dz - F_a w\Big|_{z=0} + M_a\frac{dw}{dz}\Big|_{z=0} \quad (1)$$

where w is the lateral pile deflection, and σ_{pq} and ε_{pq} are the stress and strain tensors (see Fig. 2) in the soil (summation is implied by the repetition of the indices p and q in the product of corresponding stress and strain components). The first integral represents the internal potential energy of the pile. The second and third integrals represent the internal potential

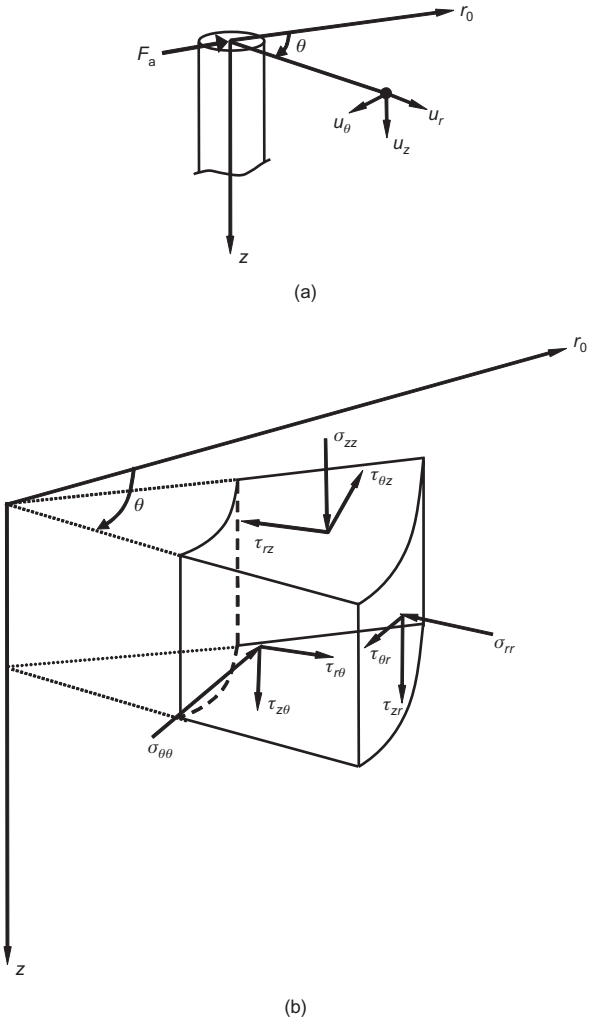

Fig. 2. (a) Displacements and (b) stresses within soil mass

energy of the continuum (note that the third integral represents the energy of the column of soil with radius r_p starting at the pile base and extending to infinity downward, while the second integral represents the energy of the soil surrounding both the pile and this column of soil). The remaining two terms represent the external potential energy.

Soil displacement

We assume the following displacement fields (Fig. 2) in the soil:

$$u_r = w(z)\phi_r(r)\cos\theta \tag{2a}$$

$$u_\theta = -w(z)\phi_\theta(r)\sin\theta \tag{2b}$$

$$u_z = 0 \tag{2c}$$

where $w(z)$ is a displacement function (with a dimension of length), varying with depth z, representing the deflection of the pile axis; $\phi_r(r)$ and $\phi_\theta(r)$ are dimensionless displacement functions varying with the radial coordinate r; and θ is the angle measured clockwise from a vertical reference section ($r = r_0$) that contains the applied force vector F_a. Equation (2c) is based on the assumption that the vertical displacement of the pile caused by the lateral load and moment applied at the pile head is negligible.

The functions $\phi_r(r)$ and $\phi_\theta(r)$ describe how the displacements within the soil mass (due to pile deflection) decrease with increasing radial distance from the pile axis. We set $\phi_r(r) = 1$ and $\phi_\theta(r) = 1$ at $r = r_p$ (this ensures compatibility at the pile/soil interface) and $\phi_r(r) = 0$ and $\phi_\theta(r) = 0$ at $r = \infty$ (this ensures that displacements in the soil decrease with increasing radial distance from the pile). Thus ϕ_r and ϕ_θ vary between 1 at the pile/soil interface and 0 at infinite radial distance from the pile.

Stress–strain–displacement relationships

The strain–displacement relationship, considering equation (2), leads to

$$\begin{bmatrix}\varepsilon_{rr}\\ \varepsilon_{\theta\theta}\\ \varepsilon_{zz}\\ \gamma_{r\theta}\\ \gamma_{rz}\\ \gamma_{\theta z}\end{bmatrix} = \begin{bmatrix} -\dfrac{\partial u_r}{\partial r}\\ -\dfrac{u_r}{r}-\dfrac{1}{r}\dfrac{\partial u_\theta}{\partial\theta}\\ -\dfrac{\partial u_z}{\partial z}\\ -\dfrac{1}{r}\dfrac{\partial u_r}{\partial\theta}-\dfrac{\partial u_\theta}{\partial r}+\dfrac{u_\theta}{r}\\ -\dfrac{\partial u_z}{\partial r}-\dfrac{\partial u_r}{\partial z}\\ -\dfrac{1}{r}\dfrac{\partial u_z}{\partial\theta}-\dfrac{\partial u_\theta}{\partial z}\end{bmatrix} = \begin{bmatrix} -w(z)\dfrac{\mathrm{d}\phi_r(r)}{\mathrm{d}r}\cos\theta\\ -w(z)\dfrac{\phi_r(r)-\phi_\theta(r)}{r}\cos\theta\\ 0\\ w(z)\left\{\dfrac{\phi_r(r)-\phi_\theta(r)}{r}+\dfrac{\mathrm{d}\phi_\theta(r)}{\mathrm{d}r}\right\}\sin\theta\\ -\dfrac{\mathrm{d}w(z)}{\mathrm{d}z}\phi_r(r)\cos\theta\\ \dfrac{\mathrm{d}w(z)}{\mathrm{d}z}\phi_\theta(r)\sin\theta\end{bmatrix} \tag{3}$$

The strains in equation (3) are related to stresses using the elastic stress–strain relationships, which allow expression of the soil potential energy density $\frac{1}{2}\sigma_{pq}\varepsilon_{pq}$ in terms of the displacement functions $w(z)$, $\phi_r(r)$ and $\phi_\theta(r)$, and the soil elastic constants λ_s and G_s (see Appendix 1). Substituting this expression for the potential energy density into equation (1), we obtain

$$\begin{aligned}\Pi = {} & \frac{1}{2}E_pI_p\int_0^{L_p}\left(\frac{\mathrm{d}^2w}{\mathrm{d}z^2}\right)^2\mathrm{d}z+\frac{\pi}{2}\int_0^\infty\int_{r_p}^\infty\Bigg[(\lambda_s+2G_s)w^2\left(\frac{\mathrm{d}\phi_r}{\mathrm{d}r}\right)^2\\ & +2\lambda_s w^2\frac{\mathrm{d}\phi_r}{\mathrm{d}r}\frac{(\phi_r-\phi_\theta)}{r}+(\lambda_s+3G_s)w^2\frac{(\phi_r-\phi_\theta)^2}{r^2}\\ & +G_s w^2\left(\frac{\mathrm{d}\phi_\theta}{\mathrm{d}r}\right)^2+2G_s w^2\frac{(\phi_r-\phi_\theta)}{r}\frac{\mathrm{d}\phi_\theta}{\mathrm{d}r}+G_s\left(\frac{\mathrm{d}w}{\mathrm{d}z}\right)^2\phi_r^2\\ & +G_s\left(\frac{\mathrm{d}w}{\mathrm{d}z}\right)^2\phi_\theta^2\Bigg]r\mathrm{d}r\mathrm{d}z+\frac{\pi}{2}r_p^2\int_{L_p}^\infty G_s\left(\frac{\mathrm{d}w}{\mathrm{d}z}\right)^2\mathrm{d}z\\ & -F_a w\Big|_{z=0}+M_a\frac{\mathrm{d}w}{\mathrm{d}z}\Big|_{z=0}\end{aligned} \tag{4}$$

Principle of minimum potential energy

A system in equilibrium exists with its potential energy at a minimum. Hence minimising the potential energy of the pile–soil system (i.e. setting the first variation of the potential energy $\delta\Pi$ equal to 0) produces the equilibrium equations. We apply $\delta\Pi = 0$ to obtain an equation of the form (see Appendix 1)

$$\begin{aligned}\delta\Pi = {} & \left[A(w)\delta w + B(w)\delta\left(\frac{\mathrm{d}w}{\mathrm{d}z}\right)\right]\\ & +\left[C(\phi_r)\delta\phi_r\right]+\left[D(\phi_\theta)\delta\phi_\theta\right]=0\end{aligned} \tag{5}$$

Since the variations $\delta w(z)$, $\delta(\mathrm{d}w/\mathrm{d}z)$, $\delta\phi_r(r)$ and $\delta\phi_\theta(r)$ of the functions $w(z)$ (and its derivative), $\phi_r(r)$ and $\phi_\theta(r)$ are independent, the terms associated with each of these variations must individually be equal to zero (i.e. $A(w)\delta w = 0$, $B(w)\delta(\mathrm{d}w/\mathrm{d}z) = 0$, $C(\phi_r)\delta\phi_r = 0$ and $D(\phi_\theta)\delta\phi_\theta = 0$) in order to satisfy the condition $\delta\Pi = 0$. The resulting equations produce the optimal functions $w_{opt}(z)$, $\phi_{r,opt}(r)$ and $\phi_{\theta,opt}(r)$ that describe the equilibrium configuration of the pile–soil system.

While considering the terms of the variation of the potential energy related to w, we do so for the following sub-domains: $0 \leqslant z \leqslant H_1$, $H_1 \leqslant z \leqslant H_2$, …, $H_{n-1} \leqslant z \leqslant L_p$, and $L_p \leqslant z < \infty$. Accordingly, w is forced to satisfy equilibrium within each of these sub-domains, and hence over the entire domain. For ϕ_r and ϕ_θ the domain over which the potential energy and its variation are calculated is $r_p \leqslant r < \infty$.

Soil displacement profiles

We first consider the variation of $\phi_r(r)$. Referring back to the equation $\delta\Pi = 0$, represented by equation (5), we first collect all the terms associated with $\delta\phi_r$ and collectively set them equal to zero to obtain

$$\begin{aligned}&\int_{r_p}^\infty\left[-m_{s1}\left(r\frac{\mathrm{d}^2\phi_r}{\mathrm{d}r^2}+\frac{\mathrm{d}\phi_r}{\mathrm{d}r}\right)+(m_{s2}+m_{s3})\frac{\mathrm{d}\phi_\theta}{\mathrm{d}r}\right.\\ &\left.+m_{s4}\frac{\phi_r}{r}-m_{s4}\frac{\phi_\theta}{r}+n_s r\phi_r\right]\delta\phi_r\mathrm{d}r\\ &+\left(m_{s1}r\frac{\mathrm{d}\phi_r}{\mathrm{d}r}+m_{s3}\phi_r-m_{s3}\phi_\theta\right)\delta\phi_r\Big|_{r_p}^\infty=0\end{aligned} \tag{6}$$

where

$$m_{s1} = (\lambda_s + 2G_s)\int_0^\infty w^2 dz = \sum_{i=1}^{n+1}(\lambda_{si} + 2G_{si})\int_{H_{i-1}}^{H_i} w_i^2 dz \tag{7}$$

$$m_{s2} = G_s\int_0^\infty w^2 dz = \sum_{i=1}^{n+1} G_{si}\int_{H_{i-1}}^{H_i} w_i^2 dz \tag{8}$$

$$m_{s3} = \lambda_s\int_0^\infty w^2 dz = \sum_{i=1}^{n+1} \lambda_{si}\int_{H_{i-1}}^{H_i} w_i^2 dz \tag{9}$$

$$m_{s4} = (\lambda_s + 3G_s)\int_0^\infty w^2 dz = \sum_{i=1}^{n+1}(\lambda_{si} + 3G_{si})\int_{H_{i-1}}^{H_i} w_i^2 dz \tag{10}$$

$$n_s = G_s\int_0^\infty \left(\frac{dw}{dz}\right)^2 dz = \sum_{i=1}^{n+1} G_{si}\int_{H_{i-1}}^{H_i} \left(\frac{dw_i}{dz}\right)^2 dz \tag{11}$$

The subscript i in the above equations refers to the ith layer of the multilayered continuum (Fig. 1); w_i represents the function $w(z)$ in the ith layer with $w_i|_{z=H_i} = w_{i+1}|_{z=H_i}$. Note that the nth (bottom) layer is split into two parts, with the part below the pile denoted by the subscript $n+1$; therefore, in the analysis, $H_n = L_p$ and $H_{n+1} \to \infty$.

The last term on the left-hand side of equation (6) is a multiple of the subtraction of the value of $\delta\phi_r$ at $r = r_p$ from the value of $\delta\phi_r$ at $r = \infty$, and is therefore identically zero for the boundary conditions of our problem ($\phi_r = 0$ at $r = \infty$ and $\phi_r = 1$ at $r = r_p$) because a known (or prescribed) ϕ_r implies that its variation $\delta\phi_r = 0$. After this term is made equal to zero, what is left is an equation of form $C(\phi_r)\delta\phi_r = 0$. The function $\phi_r(r)$ has a non-zero variation (i.e. $\delta\phi_r \neq 0$) for $r_p < r < \infty$ because ϕ_r is not known a priori in this interval, so $C(\phi_r) = 0$, which means the integrand in equation (6) must be set to zero, leading to the differential equation

$$\frac{d^2\phi_r}{dr^2} + \frac{1}{r}\frac{d\phi_r}{dr} - \left[\left(\frac{\gamma_1}{r}\right)^2 + \left(\frac{\gamma_2}{r_p}\right)^2\right]\phi_r = \frac{\gamma_3^2}{r}\frac{d\phi_\theta}{dr} - \left(\frac{\gamma_1}{r}\right)^2\phi_\theta \tag{12}$$

where the γs are dimensionless constants given by $\gamma_1^2 = m_{s4}/m_{s1}$, $(\gamma_2/r_p)^2 = n_s/m_{s1}$ and $\gamma_3^2 = (m_{s2} + m_{s3})/m_{s1}$. When solved, equation (12) yields $\phi_{r,opt}$.

We now consider the variation of $\phi_\theta(r)$. We collect the terms containing $\delta\phi_\theta$ in the equation $\delta\Pi = 0$ (equation (5)) and, proceeding similarly as for ϕ_r, we get the following governing differential equation for ϕ_θ:

$$\frac{d^2\phi_\theta}{dr^2} + \frac{1}{r}\frac{d\phi_\theta}{dr} - \left[\left(\frac{\gamma_4}{r}\right)^2 + \left(\frac{\gamma_5}{r_p}\right)^2\right]\phi_\theta = -\frac{\gamma_6^2}{r}\frac{d\phi_r}{dr} - \left(\frac{\gamma_4}{r}\right)^2\phi_r \tag{13}$$

with the following boundary conditions: $\phi_\theta = 0$ at $r = \infty$ and $\phi_\theta = 1$ at $r = r_p$, where $\gamma_4^2 = m_{s4}/m_{s2}$, $(\gamma_5/r_p)^2 = n_s/m_{s2}$, and $\gamma_6^2 = (m_{s2} + m_{s3})/m_{s2}$.

Pile displacement

Finally, we consider the variation of the function w and its derivative. We again refer back to the equation $\delta\Pi = 0$, collect all the terms associated with δw and $\delta(dw/dz)$ and equate their sum to zero, to obtain

$$\begin{aligned}
&\sum_{i=1}^{n}\int_{H_{i-1}}^{H_i}\left(E_pI_p\frac{d^4w_i}{dz^4} - 2t_i\frac{d^2w_i}{dz^2} + k_iw_i\right)\delta w_i dz \\
&+ \int_{L_p}^{\infty}\left(-2t_{n+1}\frac{d^2w_{n+1}}{dz^2} + k_nw_{n+1}\right)\delta w_{n+1} dz \\
&+ \left(E_pI_p\frac{d^3w_1}{dz^3} - 2t_1\frac{dw_1}{dz} - F_a\right)\delta w_1\Big|_{z=0} \\
&- \left(E_pI_p\frac{d^2w_1}{dz^2} - M_a\right)\delta\left(\frac{dw_1}{dz}\right)\Big|_{z=0} \\
&+ \left[-\left(E_pI_p\frac{d^3w_1}{dz^3} - 2t_1\frac{dw_1}{dz}\right)\delta w_1\Big|_{z=H_1} \right. \\
&\qquad \left. + \left(E_pI_p\frac{d^3w_2}{dz^3} - 2t_2\frac{dw_2}{dz}\right)\delta w_2\Big|_{z=H_1}\right] \\
&+ \left[E_pI_p\frac{d^2w_1}{dz^2}\delta\left(\frac{dw_1}{dz}\right)\Big|_{z=H_1} \right. \\
&\qquad \left. - E_pI_p\frac{d^2w_2}{dz^2}\delta\left(\frac{dw_2}{dz}\right)\Big|_{z=H_1}\right] + \dots . \\
&+ \left[-\left(E_pI_p\frac{d^3w_n}{dz^3} - 2t_n\frac{dw_n}{dz}\right)\delta w_n\Big|_{z=L_p} \right. \\
&\qquad \left. - 2t_{n+1}\frac{dw_{n+1}}{dz}\delta w_{n+1}\Big|_{z=L_p}\right] \\
&+ E_pI_p\frac{d^2w_n}{dz^2}\delta\left(\frac{dw_n}{dz}\right)\Big|_{z=L_p} \\
&+ 2t_{n+1}\frac{dw_{n+1}}{dz}\delta w_{n+1}\Big|_{z=\infty} = 0
\end{aligned} \tag{14}$$

where

$$t_i = \begin{cases} \dfrac{\pi}{2}G_{si}\left[\displaystyle\int_{r_p}^{\infty}(\phi_r^2 + \phi_\theta^2)\,r\,dr\right]; & i = 1, 2, \dots, n \\ \dfrac{\pi}{2}G_{sn}\left[\displaystyle\int_{r_p}^{\infty}(\phi_r^2 + \phi_\theta^2)\,r\,dr + r_p^2\right]; & i = n+1 \end{cases} \tag{15}$$

$$\begin{aligned}
k_i = \pi\Bigg[&(\lambda_{si} + 2G_{si})\int_{r_p}^{\infty} r\left(\frac{d\phi_r}{dr}\right)^2 dr + G_{si}\int_{r_p}^{\infty} r\left(\frac{d\phi_\theta}{dr}\right)^2 dr \\
&+ 2\lambda_{si}\int_{r_p}^{\infty}(\phi_r - \phi_\theta)\frac{d\phi_r}{dr}dr \\
&+ 2G_{si}\int_{r_p}^{\infty}(\phi_r - \phi_\theta)\frac{d\phi_\theta}{dr}dr \\
&+ (\lambda_{si} + 3G_{si})\int_{r_p}^{\infty}\frac{1}{r}(\phi_r - \phi_\theta)^2 dr\Bigg]
\end{aligned} \tag{16}$$

We first consider the domain below the pile, that is, $L_p \leqslant z < \infty$. The terms associated with δw and $\delta(\mathrm{d}w/\mathrm{d}z)$ in equation (14) for $L_p \leqslant z < \infty$ are equated to zero. Since the variation of $w(z)$ with depth is not known a priori within the interior of the domain $L_p < z < \infty$, $\delta w_{n+1} \neq 0$, and so the integrand in the integral between $z = L_p$ and $z = \infty$ must be equal to zero in order to satisfy equation (14). This results in the differential equation

$$2t_{n+1}\frac{\mathrm{d}^2 w_{n+1}}{\mathrm{d}z^2} - k_n w_{n+1} = 0 \tag{17}$$

The displacement in the soil must vanish for z equal to infinity. We use this as our boundary condition:

$$w_{n+1} = 0 \text{ (at } z = \infty) \tag{18}$$

The above equation implies that $\delta w_{n+1} = 0$ at $z = \infty$, making the term associated with δw at $z = \infty$ equal to zero (which is of course required to satisfy equation (14)).

The solution of equation (17) satisfying boundary condition (18) is

$$w_{n+1} = w_n|_{z=L_p} \mathrm{e}^{-\sqrt{(k_n/2t_{n+1})}(z-L_p)} \tag{19}$$

We now consider the function w for the domains $0 \leqslant z \leqslant H_1$, $H_1 \leqslant z \leqslant H_2$, …, $H_{n-1} \leqslant z \leqslant L_p$. The terms containing δw and $\delta(\mathrm{d}w/\mathrm{d}z)$ in equation (14) are equated to zero for each domain. Considering the integrals associated with each individual layer (or each domain $H_{i-1} < z < H_i$), the integrand for each of these integrals must equal zero, because $\delta w_i \neq 0$ (as the function $w_i(z)$ within the domains is not known a priori). This gives us the differential equation for the ith layer, which, expressed in terms of normalised depth $\tilde{z} = z/L_p$ and displacement $\tilde{w} = w/L_p$, is given by

$$\frac{\mathrm{d}^4\tilde{w}_i}{\mathrm{d}\tilde{z}^4} - 2\tilde{t}_i\frac{\mathrm{d}^2\tilde{w}_i}{\mathrm{d}\tilde{z}^2} + \tilde{k}_i\tilde{w}_i = 0 \tag{20}$$

The terms associated with the boundaries (i.e. $z = H_i$) of each domain in equation (14) must also each be equal to zero. For each boundary, there are two terms: one multiplying δw_i and another multiplying $\delta(\mathrm{d}w_i/\mathrm{d}z)$. Setting each separately equal to zero yields the boundary conditions for the differential equations represented by equation (20). These terms can be seen to be a product of an expression and the variation of the displacement or of its derivative. If the displacement or its derivative is specified at the boundary, then its variation is equal to zero; otherwise, the expression multiplying the variation of the displacement or of its derivative is equal to zero. The boundary conditions at the pile head ($z = \tilde{z} = 0$) are

$$\tilde{w}_1 = \text{constant} \tag{21a}$$

or

$$\frac{\mathrm{d}^3\tilde{w}_1}{\mathrm{d}\tilde{z}^3} - 2\tilde{t}_1\frac{\mathrm{d}\tilde{w}_1}{\mathrm{d}\tilde{z}} - \tilde{F}_a = 0 \tag{21b}$$

and

$$\frac{\mathrm{d}\tilde{w}_1}{\mathrm{d}\tilde{z}} = \text{constant} \tag{21c}$$

or

$$\frac{\mathrm{d}^2\tilde{w}_1}{\mathrm{d}\tilde{z}^2} - \tilde{M}_a = 0 \tag{21d}$$

At the interface between any two layers ($z = H_i$ or $\tilde{z} = \tilde{H}_i$),

$$\tilde{w}_i = \tilde{w}_{i+1} \tag{22a}$$

$$\frac{\mathrm{d}\tilde{w}_i}{\mathrm{d}\tilde{z}} = \frac{\mathrm{d}\tilde{w}_{i+1}}{\mathrm{d}\tilde{z}} \tag{22b}$$

$$\frac{\mathrm{d}^3\tilde{w}_i}{\mathrm{d}\tilde{z}^3} - 2\tilde{t}_i\frac{\mathrm{d}\tilde{w}_i}{\mathrm{d}\tilde{z}} = \frac{\mathrm{d}^3\tilde{w}_{i+1}}{\mathrm{d}\tilde{z}^3} - 2\tilde{t}_{i+1}\frac{\mathrm{d}\tilde{w}_{i+1}}{\mathrm{d}\tilde{z}} \tag{22c}$$

$$\frac{d^2\tilde{w}_i}{d\tilde{z}^2} = \frac{d^2\tilde{w}_{i+1}}{d\tilde{z}^2} \tag{22d}$$

At the pile base ($z = L_p$ or $\tilde{z} = 1$), the boundary conditions are

$$\tilde{w}_n = \text{constant} \tag{23a}$$

or

$$\frac{\mathrm{d}^3\tilde{w}_n}{\mathrm{d}\tilde{z}^3} - 2\tilde{t}_n\frac{\mathrm{d}\tilde{w}_n}{\mathrm{d}\tilde{z}} = -2\tilde{t}_{n+1}\frac{\mathrm{d}\tilde{w}_{n+1}}{\mathrm{d}\tilde{z}} \tag{23b}$$

and

$$\frac{\mathrm{d}\tilde{w}_n}{\mathrm{d}\tilde{z}} = \text{constant} \tag{23c}$$

or

$$\frac{\mathrm{d}^2\tilde{w}_n}{\mathrm{d}\tilde{z}^2} = 0 \tag{23d}$$

Equation (23b) is further simplified and expressed solely in terms of $\tilde{w}_n$ by differentiating w_{n+1} in equation (19) with respect to z, normalising the expression, and then substituting it back into equation (23b) to yield

$$\frac{\mathrm{d}^3\tilde{w}_n}{\mathrm{d}\tilde{z}^3} - 2\tilde{t}_n\frac{\mathrm{d}\tilde{w}_n}{\mathrm{d}\tilde{z}} - \sqrt{2\tilde{k}_n\tilde{t}_{n+1}}\tilde{w}_n = 0 \tag{23b′}$$

The dimensionless terms in the above equations are defined as $\tilde{t}_i = t_i L_p^2/E_p I_p$, $\tilde{k}_i = k_i L_p^4/E_p I_p$, $\tilde{F}_a = F_a L_p^2/E_p I_p$, $\tilde{M}_a = M_a L_p/E_p I_p$ and $\tilde{H}_i = H_i/L_p$.

The governing differential equation for the pile (equation (20)) resembles that of an Euler–Bernoulli beam resting on an elastic foundation (the soil mass). The parameter k_i (with dimensions of FL^{-2}, where F = force and L = length) is related to the modulus of subgrade reaction (or to the 'spring constant' proposed by Winkler, 1867) and determines the portion of the soil resistance due to compressive stresses in the elastic medium (Fig. 3). On the other hand, the

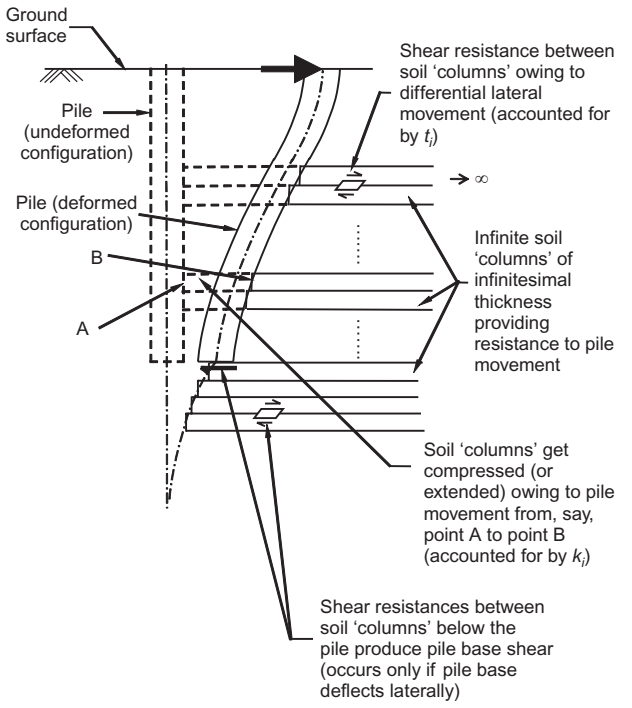

Fig. 3. Illustration of the two sources of soil resistance: soil compression and shear

parameter t_i (with dimension of F) determines the fraction of the soil resistance due to the shear stresses that develop between soil layers of infinitesimal thickness displaced differentially in the lateral direction (Vlasov & Leont'ev, 1966).

The boundary conditions (equations (22a)–(22d)) at the interface of any two layers ($\tilde{z} = \tilde{H}_i$) ensure the continuity of pile deflection, slope of the deflection curve ($= \mathrm{d}w_i/\mathrm{d}z$), bending moment ($= E_\mathrm{p}I_\mathrm{p}(\mathrm{d}^2w_i/\mathrm{d}z^2)$) and shear force ($= E_\mathrm{p}I_\mathrm{p}(\mathrm{d}^3w_i/\mathrm{d}z^3) - 2t_i(\mathrm{d}w_i/\mathrm{d}z)$) (the shear force has contributions from both pile flexure and soil deformation). At the pile head ($\tilde{z} = 0$) the shear force equals the applied force (equation (21b)), and either the slope of the pile deflection curve is a known constant (equation (21c)) (this boundary condition is generally used with the value of slope taken equal to zero when fixed-head conditions are used to idealise the case of a pile that is part of a group of piles joined at the head by a cap) or the pile bending moment is equal to the applied moment (equation (21d)) (free-head case). Equation (21a) must be used in the analysis instead of equation (21b) to estimate the magnitude of an applied force required to produce a given (known) head deflection. Similarly, if, for both the free- and fixed-head cases, it becomes necessary to estimate the magnitude of an applied moment that produces a given (known) slope at the head, equation (21c) must be used.

At the pile base ($\tilde{z} = 1$), either the pile deflection is set (equation (23a)) (used for the ideal fixed-base case, for which the deflection is taken equal to zero, which may be used with satisfactory results if the pile is socketed into a very firm layer, like hard rock) or the shear force at a section infinitesimally above the pile base is equal to that infinitesimally below (equation (23b′)) (free-base case). The other boundary condition active at the pile base is that either the slope is a constant (equation (23c)) (assumed to be zero for the fixed-base case) or the pile bending moment is zero (equation (23d)) (free-base case).

Expressions for the γs in terms of dimensionless deflections

The γs appearing in equations (12) and (13) are expressed in terms of the dimensionless pile deflection and slope as follows:

$$\gamma_1 = \sqrt{\frac{\sum_{i=1}^{n}(\lambda_{si}+3G_{si})\int_{\tilde{H}_{i-1}}^{\tilde{H}_i}\tilde{w}_i^2\,\mathrm{d}\tilde{z} + (\lambda_{sn}+3G_{sn})\sqrt{\frac{\tilde{t}_{n+1}}{2\tilde{k}_n}}\tilde{w}_n^2|_{\tilde{z}=1}}{\sum_{i=1}^{n}(\lambda_{si}+2G_{si})\int_{\tilde{H}_{i-1}}^{\tilde{H}_i}\tilde{w}_i^2\,\mathrm{d}\tilde{z} + (\lambda_{sn}+2G_{sn})\sqrt{\frac{\tilde{t}_{n+1}}{2\tilde{k}_n}}\tilde{w}_n^2|_{\tilde{z}=1}}} \tag{24}$$

$$\gamma_2 = \sqrt{\frac{1}{\psi^2}\frac{\sum_{i=1}^{n}G_{si}\int_{\tilde{H}_{i-1}}^{\tilde{H}_i}\left(\frac{\mathrm{d}\tilde{w}_i}{\mathrm{d}\tilde{z}}\right)^2\mathrm{d}\tilde{z} + G_{sn}\sqrt{\frac{\tilde{k}_n}{8\tilde{t}_{n+1}}}\tilde{w}_n^2|_{\tilde{z}=1}}{\sum_{i=1}^{n}(\lambda_{si}+2G_{si})\int_{\tilde{H}_{i-1}}^{\tilde{H}_i}\tilde{w}_i^2\,\mathrm{d}\tilde{z} + (\lambda_{sn}+2G_{sn})\sqrt{\frac{\tilde{t}_{n+1}}{2\tilde{k}_n}}\tilde{w}_n^2|_{\tilde{z}=1}}} \tag{25}$$

$$\gamma_3 = \sqrt{\frac{\sum_{i=1}^{n}(\lambda_{si}+G_{si})\int_{\tilde{H}_{i-1}}^{\tilde{H}_i}\tilde{w}_i^2\,\mathrm{d}\tilde{z} + (\lambda_{sn}+G_{sn})\sqrt{\frac{\tilde{t}_{n+1}}{2\tilde{k}_n}}\tilde{w}_n^2|_{\tilde{z}=1}}{\sum_{i=1}^{n}(\lambda_{si}+2G_{si})\int_{\tilde{H}_{i-1}}^{\tilde{H}_i}\tilde{w}_i^2\,\mathrm{d}\tilde{z} + (\lambda_{sn}+2G_{sn})\sqrt{\frac{\tilde{t}_{n+1}}{2\tilde{k}_n}}\tilde{w}_n^2|_{\tilde{z}=1}}} \tag{26}$$

$$\gamma_4 = \sqrt{\frac{\sum_{i=1}^{n}(\lambda_{si}+3G_{si})\int_{\tilde{H}_{i-1}}^{\tilde{H}_i}\tilde{w}_i^2\,\mathrm{d}\tilde{z} + (\lambda_{sn}+3G_{sn})\sqrt{\frac{\tilde{t}_{n+1}}{2\tilde{k}_n}}\tilde{w}_n^2|_{\tilde{z}=1}}{\sum_{i=1}^{n}G_{si}\int_{\tilde{H}_{i-1}}^{\tilde{H}_i}\tilde{w}_i^2\,\mathrm{d}\tilde{z} + G_{sn}\sqrt{\frac{\tilde{t}_{n+1}}{2\tilde{k}_n}}\tilde{w}_n^2|_{\tilde{z}=1}}} \tag{27}$$

$$\gamma_5 = \sqrt{\frac{1}{\psi^2}\frac{\sum_{i=1}^{n}G_{si}\int_{\tilde{H}_{i-1}}^{\tilde{H}_i}\left(\frac{\mathrm{d}\tilde{w}_i}{\mathrm{d}\tilde{z}}\right)^2\mathrm{d}\tilde{z} + G_{sn}\sqrt{\frac{\tilde{k}_n}{8\tilde{t}_{n+1}}}\tilde{w}_n^2|_{\tilde{z}=1}}{\sum_{i=1}^{n}G_{si}\int_{\tilde{H}_{i-1}}^{\tilde{H}_i}\tilde{w}_i^2\,\mathrm{d}\tilde{z} + G_{sn}\sqrt{\frac{\tilde{t}_{n+1}}{2\tilde{k}_n}}\tilde{w}_n^2|_{\tilde{z}=1}}} \tag{28}$$

$$\gamma_6 = \sqrt{\frac{\sum_{i=1}^{n}(\lambda_{si}+G_{si})\int_{\tilde{H}_{i-1}}^{\tilde{H}_i}\tilde{w}_i^2\,\mathrm{d}\tilde{z} + (\lambda_{sn}+G_{sn})\sqrt{\frac{\tilde{t}_{n+1}}{2\tilde{k}_n}}\tilde{w}_n^2|_{\tilde{z}=1}}{\sum_{i=1}^{n}G_{si}\int_{\tilde{H}_{i-1}}^{\tilde{H}_i}\tilde{w}_i^2\,\mathrm{d}\tilde{z} + G_{sn}\sqrt{\frac{\tilde{t}_{n+1}}{2\tilde{k}_n}}\tilde{w}_n^2|_{\tilde{z}=1}}} \tag{29}$$

where $\psi = L_\mathrm{p}/r_\mathrm{p}$. These expressions can be directly used in the computations.

ANALYTICAL SOLUTION FOR PILE DEFLECTION

The general solution of equation (20) is given by

$$\tilde{w}_i(\tilde{z}) = C_1^{(i)}\Phi_1 + C_2^{(i)}\Phi_2 + C_3^{(i)}\Phi_3 + C_4^{(i)}\Phi_4 \tag{30}$$

where $C_1^{(i)}$, $C_2^{(i)}$, $C_3^{(i)}$ and $C_4^{(i)}$ are integration constants (for the ith layer), and Φ_1, Φ_2, Φ_3 and Φ_4 are individual solutions (functions of $\tilde{z}$) of the differential equation. The functions Φ_1, Φ_2, Φ_3 and Φ_4 are standard trigonometric or hyperbolic functions that arise in the solution of the linear ordinary differential equations (Table 1). The integration constants for each layer can be determined using the boundary conditions. The boundary conditions given in equations (21)–(23) lead to a system of linear algebraic equations (see Appendix 2) of the form

$$[\Theta][\mathrm{C}] = [\mathrm{F}] \tag{31}$$

where $[\Theta]_{4n\times 4n}$ is a matrix containing the functions Φ_1, Φ_2, Φ_3 and Φ_4 calculated at the boundaries of the soil layers, $[\mathrm{C}]_{4n\times 1}$ is the vector of unknown integration constants of all the layers, and $[\mathrm{F}]_{4n\times 1}$ is the right-hand side vector containing the applied forces and/or displacements (the subscript $4n$ denotes the number of equations, which is four times the number of soil layers). Simultaneous solution of the system of equations represented by equation (31) produces the values of the integration constants $C_1^{(i)}$, $C_2^{(i)}$, $C_3^{(i)}$ and $C_4^{(i)}$, which, when substituted in equation (30), produce the particular solution of pile deflection (i.e. the pile deflection profile) for a given set of boundary conditions and applied loads. The slope of the deflected pile axis, and the bending moment and shear force in the pile, can be obtained as a function of depth by successively differentiating equation (30) and using the values of the integration constants.

FINITE DIFFERENCE SOLUTION FOR SOIL DISPLACEMENTS

The differential equations (12) and (13) for ϕ_r and ϕ_θ are solved using the FD method. The equations are interdependent and must, as a result, be solved simultaneously. Using the central-difference scheme, equations (12) and (13) can be respectively written as

Table 1. Functions in equation (30) for piles crossing multiple soil layers

Relative magnitudes of $\tilde{k}$ and $\tilde{t}$	Constants a and b		Functions and their derivatives*	Individual solutions of equation (20)			
	a	b		Φ_1	Φ_2	Φ_3	Φ_4
$\tilde{k} > \tilde{t}^2$	$\sqrt{\frac{1}{2}(\sqrt{\tilde{k}^2 + \tilde{t}^2} + \tilde{k})}$	$\sqrt{\frac{1}{2}(\sqrt{\tilde{k}^2 + \tilde{t}^2} - \tilde{k})}$	Φ Φ' Φ'' Φ'''	$\sinh a\tilde{z} \cos b\tilde{z}$ $a\Phi_2 - b\Phi_4$ $(a^2 - b^2)\Phi_1$ $-2ab\Phi_3$ $a(a^2 - 3b^2)\Phi_2 + b(b^2 - 3a^2)\Phi_4$	$\cosh a\tilde{z} \cos b\tilde{z}$ $a\Phi_1 - b\Phi_3$ $(a^2 - b^2)\Phi_2$ $-2ab\Phi_4$ $a(a^2 - 3b^2)\Phi_1 + b(b^2 - 3a^2)\Phi_3$	$\cosh a\tilde{z} \sin b\tilde{z}$ $a\Phi_4 + b\Phi_2$ $(a^2 - b^2)\Phi_3$ $+2ab\Phi_1$ $a(a^2 - 3b^2)\Phi_4 - b(b^2 - 3a^2)\Phi_2$	$\sinh a\tilde{z} \sin b\tilde{z}$ $a\Phi_3 + b\Phi_1$ $(a^2 - b^2)\Phi_4$ $+2ab\Phi_2$ $a(a^2 - 3b^2)\Phi_3 - b(b^2 - 3a^2)\Phi_1$
$\tilde{k} < \tilde{t}^2$	$\sqrt{\tilde{t} + \sqrt{(\tilde{t}^2 - \tilde{k})}}$	$\sqrt{\tilde{t} - \sqrt{(\tilde{t}^2 - \tilde{k})}}$	Φ Φ' Φ'' Φ'''	$\sinh a\tilde{z}$ $a\Phi_2$ $a^2\Phi_1$ $a^3\Phi_2$	$\cosh a\tilde{z}$ $a\Phi_1$ $a^2\Phi_2$ $a^3\Phi_1$	$\sinh b\tilde{z}$ $b\Phi_4$ $b^2\Phi_3$ $b^3\Phi_4$	$\cosh b\tilde{z}$ $b\Phi_3$ $b^2\Phi_4$ $b^3\Phi_3$

*Prime (′) indicates differentiation.

$$\frac{\phi_r^{j+1} - 2\phi_r^j + \phi_r^{j-1}}{\Delta r^2} + \frac{1}{r_j}\frac{\phi_r^{j+1} - \phi_r^{j-1}}{2\Delta r} - \left[\left(\frac{\gamma_1}{r_j}\right)^2 + \left(\frac{\gamma_2}{r_p}\right)^2\right]\phi_r^j = \frac{\gamma_3^2}{r_j}\frac{\phi_\theta^{j+1} - \phi_\theta^{j-1}}{2\Delta r} - \left(\frac{\gamma_1}{r_j}\right)^2\phi_\theta^j \tag{32}$$

$$\frac{\phi_\theta^{j+1} - 2\phi_\theta^j + \phi_\theta^{j-1}}{\Delta r^2} + \frac{1}{r_j}\frac{\phi_\theta^{j+1} - \phi_\theta^{j-1}}{2\Delta r} - \left[\left(\frac{\gamma_4}{r_j}\right)^2 + \left(\frac{\gamma_5}{r_p}\right)^2\right]\phi_\theta^j = -\frac{\gamma_6^2}{r_j}\frac{\phi_r^{j+1} - \phi_r^{j-1}}{2\Delta r} - \left(\frac{\gamma_4}{r_j}\right)^2\phi_r^j \tag{33}$$

where j represents the jth node, which is at a radial distance r_j from the pile axis; and Δr is the distance between consecutive nodes (discretisation length). The total number of discretised nodes m should be sufficiently large that the infinite domain in the radial direction can be adequately modelled (Fig. 4). The discretisation length Δr should be sufficiently small to maintain a satisfactory level of accuracy.

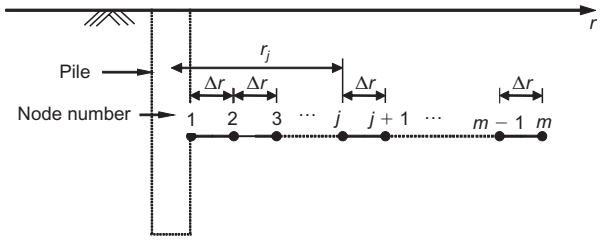

Fig. 4. Finite difference discretisation for ϕ_r and ϕ_θ

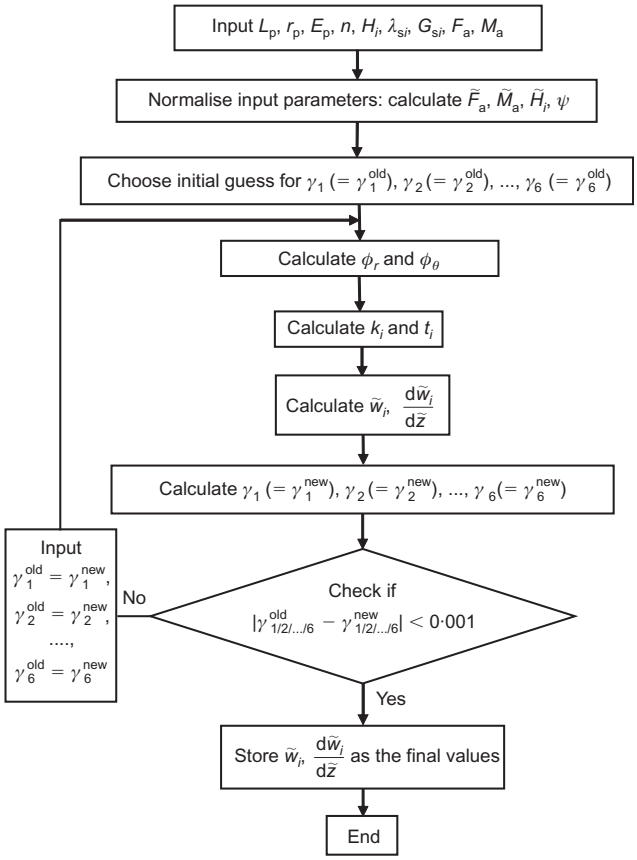

Fig. 5. Solution flow chart

Equation (32), along with the boundary conditions $\phi_r^{(1)} = 1$ (at $r = r_p$) and $\phi_r^{(m)} = 0$ (at $r = \infty$), is applied to the discretised nodes, yielding the equation

$$\begin{bmatrix} 1 & 0 & 0 & \cdots & & & & \cdots & 0 \\ 0 & K_{2,2}^{\phi_r} & K_{2,3}^{\phi_r} & 0 & \cdots & & & \cdots & 0 \\ 0 & K_{3,2}^{\phi_r} & K_{3,3}^{\phi_r} & K_{3,4}^{\phi_r} & 0 & \cdots & & \cdots & 0 \\ 0 & 0 & K_{4,3}^{\phi_r} & K_{4,4}^{\phi_r} & K_{4,5}^{\phi_r} & 0 & \cdots & \cdots & 0 \\ \vdots & & \ddots & \ddots & \ddots & \ddots & \ddots & \cdots & \vdots \\ 0 & \cdots & \cdots & 0 & K_{j,j-1}^{\phi_r} & K_{j,j}^{\phi_r} & K_{j,j+1}^{\phi_r} & \cdots & 0 \\ \vdots & & & & \ddots & \ddots & \ddots & \ddots & \vdots \\ 0 & \cdots & & & \cdots & 0 & K_{m-2,m-3}^{\phi_r} & K_{m-2,m-2}^{\phi_r} & K_{m-2,m-1}^{\phi_r} & 0 \\ 0 & \cdots & & & & \cdots & 0 & K_{m-1,m-2}^{\phi_r} & K_{m-1,m-1}^{\phi_r} & 0 \\ 0 & \cdots & & & & & \cdots & 0 & 0 & 1 \end{bmatrix} \begin{bmatrix} \phi_r^{(1)} \\ \phi_r^{(2)} \\ \phi_r^{(3)} \\ \phi_r^{(4)} \\ \vdots \\ \phi_r^{(j)} \\ \vdots \\ \phi_r^{(m-2)} \\ \phi_r^{(m-1)} \\ \phi_r^{(m)} \end{bmatrix} = \begin{bmatrix} 1 \\ F_2^{\phi_r} \\ F_3^{\phi_r} \\ F_4^{\phi_r} \\ \vdots \\ F_j^{\phi_r} \\ \vdots \\ F_{m-2}^{\phi_r} \\ F_{m-1}^{\phi_r} \\ 0 \end{bmatrix} \tag{34}$$

The non-zero elements of the left-hand side matrix $[K^{\phi_r}]_{m\times m}$ in the above equation are given by

$$K_{j,j-1}^{\phi_r} = \frac{1}{\Delta r^2} - \frac{1}{2r_j\Delta r} \tag{35}$$

$$K_{j,j}^{\phi_r} = -\frac{2}{\Delta r^2} - \left[\left(\frac{\gamma_1}{r_j}\right)^2 + \left(\frac{\gamma_2}{r_p}\right)^2\right] \tag{36}$$

$$K_{j,j+1}^{\phi_r} = \frac{1}{\Delta r^2} + \frac{1}{2r_j\Delta r} \tag{37}$$

in which the subscript j is valid for nodes 2 to $m-1$, with the exception that $K_{2,1}^{\phi_r} = 0$ and $K_{m-1,m}^{\phi_r} = 0$ (as is evident from equation (34)).

The elements of the right-hand side vector $\{F^{\phi_r}\}_{m\times 1}$ in equation (34) are given by

$$F_j^{\phi_r} = \frac{\gamma_3^2}{r_j}\frac{\phi_\theta^{j+1} - \phi_\theta^{j-1}}{2\Delta r} - \left(\frac{\gamma_1}{r_j}\right)^2\phi_\theta^j \tag{38}$$

where j represents nodes 3 through $m-2$. The elements corresponding to node 2 and $m-1$ are given by:

$$F_2^{\phi_r} = -\frac{1}{\Delta r^2} + \frac{1}{2r_2\Delta r} + \frac{\gamma_3^2}{r_2}\frac{\phi_\theta^{(3)} - 1}{2\Delta r} - \left(\frac{\gamma_1}{r_2}\right)^2\phi_\theta^{(2)} \tag{39}$$

$$F_{m-1}^{\phi_r} = \frac{\gamma_3^2}{r_{m-1}}\frac{-\phi_\theta^{m-2}}{2\Delta r} - \left(\frac{\gamma_1}{r_{m-1}}\right)^2\phi_\theta^{m-1} \tag{40}$$

Using equation (33) and the boundary conditions that $\phi_\theta^{(1)} = 1$ (at $r = r_p$) and $\phi_\theta^{(m)} = 0$ (at $r = \infty$), a matrix equation (similar to equation (34)) for ϕ_θ can also be formed for the discretised nodes:

$$[K^{\phi_\theta}]\{\phi_\theta\} = \{F^{\phi_\theta}\} \tag{41}$$

The number and positioning of the non-zero elements of $[K^{\phi_\theta}]_{m\times m}$ in equation (41) are exactly the same as that of $[K^{\phi_r}]_{m\times m}$ of equation (34). The expressions of the off-diagonal elements of $[K^{\phi_\theta}]_{m\times m}$ and $[K^{\phi_r}]_{m\times m}$ are also the same (i.e. $K_{p,q}^{\phi_r} = K_{p,q}^{\phi_\theta}$ for $p \neq q$). The diagonal elements of $[K^{\phi_\theta}]_{m\times m}$ for $j = 2$ to $m-1$ are given by

$$K_{j,j}^{\phi_r} = -\frac{2}{\Delta r^2} - \left[\left(\frac{\gamma_4}{r_j}\right)^2 + \left(\frac{\gamma_5}{r_p}\right)^2\right] \tag{42}$$

The structure of $\{F^{\phi_\theta}\}_{m\times 1}$ in equation (41) is also similar to $\{F^{\phi_r}\}_{m\times 1}$ of equation (34) with $F_1^{\phi_\theta} = 1$ and $F_m^{\phi_\theta} = 0$. The remaining elements of $\{F^{\phi_\theta}\}_{m\times 1}$ are given by

$$F_j^{\phi_\theta} = -\frac{\gamma_6^2}{r_j}\frac{\phi_r^{j+1} - \phi_r^{j-1}}{2\Delta r} - \left(\frac{\gamma_4}{r_j}\right)^2\phi_r^j \tag{43}$$

$$(j = 3, 4, \ \ldots, m-2)$$

$$F_2^{\phi_\theta} = -\frac{1}{\Delta r^2} + \frac{1}{2r_2\Delta r} - \frac{\gamma_6^2}{r_2}\frac{\phi_r^{(3)} - 1}{2\Delta r} - \left(\frac{\gamma_4}{r_2}\right)^2\phi_r^{(2)} \tag{44}$$

$$F_{m-1}^{\phi_\theta} = -\frac{\gamma_6^2}{r_{m-1}}\frac{-\phi_r^{m-2}}{2\Delta r} - \left(\frac{\gamma_4}{r_{m-1}}\right)^2\phi_r^{m-1} \tag{45}$$

Since the right-hand side vectors $\{F^{\phi_r}\}_{m\times 1}$ and $\{F^{\phi_\theta}\}_{m\times 1}$ contain the unknowns ϕ_θ and ϕ_r, iterations are necessary to obtain their values. An initial estimate of ϕ_r^j is made and given as input to $\{F^{\phi_\theta}\}$, and ϕ_θ^j is determined by solving equation (41). The ϕ_θ^j values are then given as input to $\{F^{\phi_r}\}$ to obtain ϕ_r^j from equation (34). The newly obtained values of ϕ_r^j are again used to obtain new values of ϕ_θ^j, and the iterations are continued until convergence is reached. The criteria $\frac{1}{m}\sum_{j=1}^{m}\left|\phi_r^{j\,\text{previous}} - \phi_r^{j\,\text{current}}\right| \leqslant 10^{-6}$ and $\frac{1}{m}\sum_{j=1}^{m}\left|\phi_\theta^{j\,\text{previous}} - \phi_\theta^{j\,\text{current}}\right| \leqslant 10^{-6}$ are used (a stringent value of 10^{-6} is used because this iterative solution scheme is central to another set of iterations described next) to ensure that accurate values of ϕ_r and ϕ_θ are obtained.

SOLUTION ALGORITHM

In order to obtain pile deflections by solving equation (20), the soil parameters k_i and t_i must be known. However, these soil parameters depend on ϕ_r and ϕ_θ, which are not known a priori. Hence an iterative algorithm (separate from the iterations between ϕ_r and ϕ_θ described in the previous section) is necessary to solve the problem. First, initial guesses for γ_1 to γ_6 are made, and for these assumed values ϕ_r and ϕ_θ are determined using the iterative technique described in the previous section. Using the calculated values of ϕ_r and ϕ_θ, k_i and t_i are calculated by numerical integrations (with Δr of Fig. 4 as the step length). Using the values of k_i and t_i, the pile deflection is calculated. From the calculated values of pile deflection and slope of the deformed pile, γ_1 to γ_6 are obtained. The new values of γ_1 to γ_6 are then used to recalculate ϕ_r and ϕ_θ, and so on. The entire process is repeated until convergence on each of the γs is attained. The tolerance limit prescribed on the γs between the pth and $(p+1)$th iteration is $|\gamma_{1/2/\ldots/6}^{(p+1)} - \gamma_{1/2/\ldots/6}^{(p)}| < 0{\cdot}001$. The details of the solution steps are given in the form of a flow chart in Fig. 5. We chose an initial guess of 'one' for all the γs, but any other

choice would produce results with the same level of accuracy at approximately the same computation time.

BENEFITS OF THE PRESENT ANALYSIS

This analysis is an improvement over the analysis of Sun (1994) for laterally loaded piles in homogeneous soil on at least two accounts: (a) our assumption of the displacement field is more general and more realistic than that assumed by Sun (1994), who chose $\phi_r(r) = \phi_\theta(r) = \phi(r)$ for both the displacements u_r and u_θ (equation (2)); and (b) we obtained solutions for a multilayered soil, whereas the solution of Sun (1994) is valid only for a single soil layer.

The need for an improved form for the displacement field (equation (2)) arises from the fact that the displacement assumption of Sun (1994) produces zero displacement in the soil mass perpendicular to the direction of the applied force F_a (Fig. 6). Consequently, the resultant displacement vector $\boldsymbol{u} = \boldsymbol{e}_r u_r + \boldsymbol{e}_\theta u_\theta$ ($\boldsymbol{e}_r$ and $\boldsymbol{e}_\theta$ are the unit basis vectors in the radial and tangential directions respectively) at any point within the soil mass is forced to be parallel to the applied force F_a. Thus the displacement field in the soil mass (which, in general, has a component perpendicular to the direction of F_a) is artificially constrained, the normal strain in the circumferential direction $\varepsilon_{\theta\theta}$ (equation (3)) becomes zero, and the pile response is stiffer than what it is in reality. In fact, Guo & Lee (2001) found that the Sun (1994) analysis produces unreliable pile response, particularly if the Poisson's ratio of soil is greater than 0·3. This artificially stiff pile response is not observed in our analysis. To illustrate this point, we present below two examples comparing the results of our analysis, the analysis based on the displacement assumption of Sun (1994), and 3D FE analysis.

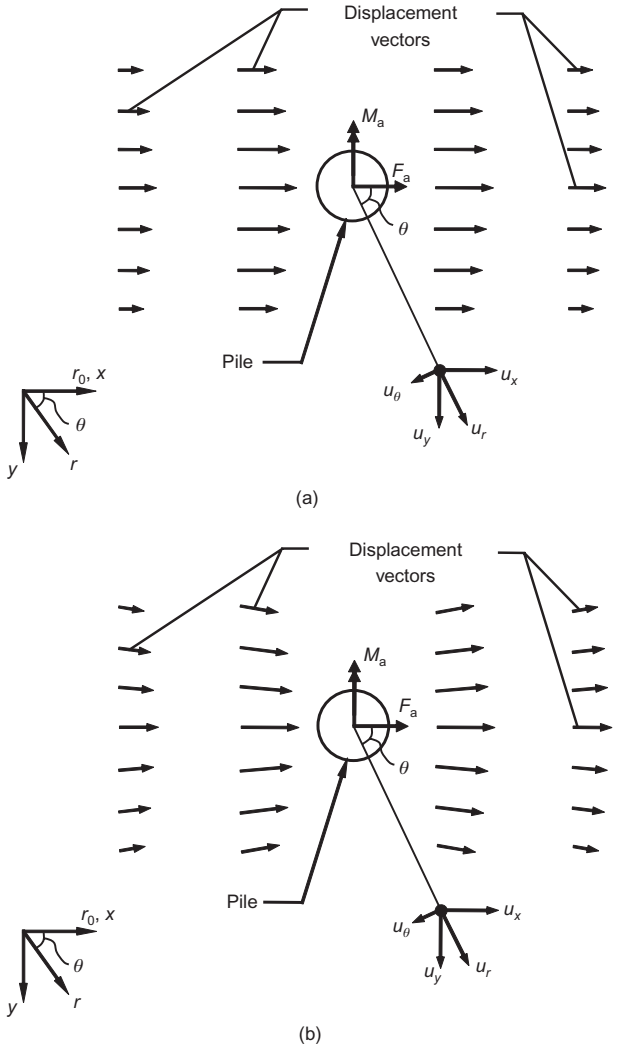

Fig. 6. Displacement field in soil: (a) according to Sun (1994) assumption; (b) according to assumption made in this paper

We consider as an illustration of use of the analysis a 15 m long drilled shaft, with a diameter of 0·6 m and pile modulus $E_p = 24 \times 10^6$ kN/m^2, embedded in a four-layer soil deposit with $H_1 = 2{\cdot}0$ m, $H_2 = 5{\cdot}0$ m, and $H_3 = 8{\cdot}3$ m; $E_{s1} = 20$ MPa, $E_{s2} = 35$ MPa, $E_{s3} = 50$ MPa and $E_{s4} = 80$ MPa; $\nu_{s1} = 0{\cdot}35$, $\nu_{s2} = 0{\cdot}25$, $\nu_{s3} = 0{\cdot}2$ and $\nu_{s4} = 0{\cdot}15$ (E_{si} and ν_{si} are the soil Young's modulus and Poisson's ratio for the ith layer; E_{si} and ν_{si} are related to λ_{si} and G_{si} by $\lambda_{si} = E_{si}\nu_{si}/(1+\nu_{si})(1-2\nu_{si})$ and $G_{si} = E_{si}/2(1+\nu_{si})$). A horizontal force $F_a = 300$ kN acts on the pile. The pile head and base are free to deflect and rotate. Fig. 7 shows the pile deflection profile obtained using our analysis, the analysis based on the displacement assumption of Sun (1994), and a 3D finite element analysis (FEA). The pile response obtained from our analysis closely matches that of the 3D FEA (a difference of 9·6% in the head deflection was observed between our analysis and the FEA); the analysis of Sun (1994) produces a stiffer pile response.

Next, we consider a large-diameter drilled shaft, 40 m long, with a diameter of 1·7 m and $E_p = 25 \times 10^6$ kPa, embedded in a four-layer soil profile with $H_1 = 1{\cdot}5$ m, $H_2 = 3{\cdot}5$ m, and $H_3 = 8{\cdot}5$ m; $E_{s1} = 20$ MPa, $E_{s2} = 25$ MPa, $E_{s3} = 40$ MPa and $E_{s4} = 80$ MPa; $\nu_{s1} = 0{\cdot}35$, $\nu_{s2} = 0{\cdot}3$, $\nu_{s3} = 0{\cdot}25$ and $\nu_{s4} = 0{\cdot}2$. A 3000 kN force acts at the pile head, which is free to deflect and rotate. Fig. 8 shows the pile deflection profiles, as obtained from our analysis, the analysis based on the displacement assumption of Sun (1994), and 3D FEA. As before, our results match those of the FEA more closely than the results based on the Sun (1994) assumption; the difference in the head deflection obtained from our analysis and FEA is 6·6%.

The 3D FE analyses were performed using ABAQUS. The domain for these analyses can be visualised as a cylinder of soil mass containing the pile at its centre as a concentric cylinder. The top (horizontal) surface of the soil cylinder was flush with the pile head, and the bottom (horizontal) surface was located at a finite distance below the pile base (thus the soil mass below the pile base participating in the pile–soil interaction was incorporated in the analysis). The horizontal force F_a (acting at the pile head) was applied as a uniformly distributed shear stress (i.e. force per unit pile cross-section area) acting on the pile-head surface (the

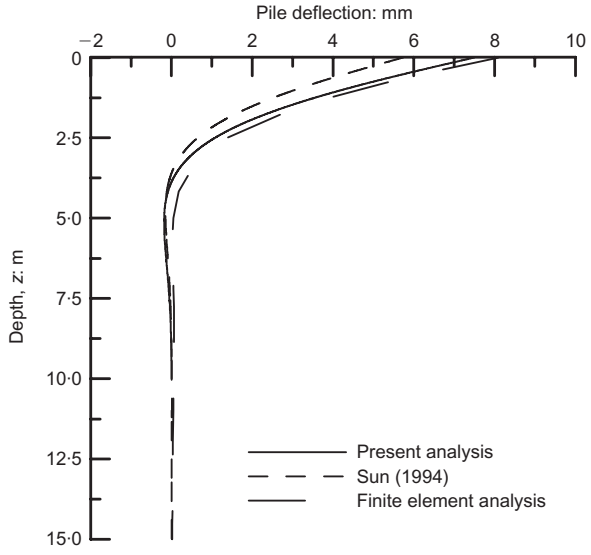

Fig. 7. Deflection profile of a 15 m long pile

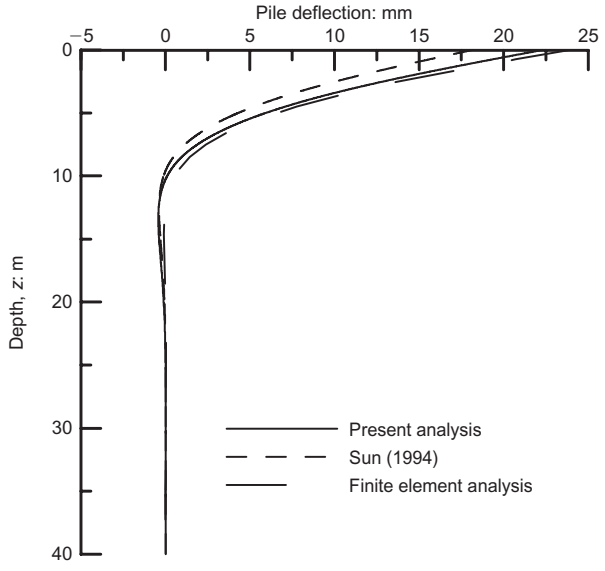

Fig. 8. Deflection profile of a 40 m long drilled shaft

distributed shear stress multiplied by the pile cross-section area produced F_a). The vertical plane passing through the pile axis parallel to F_a is a plane of symmetry (the plane contains the F_a vector) and divides the cylindrical domain into two equal and symmetrical halves. Only one such half was used as the analysis domain. Different boundary conditions were prescribed at different boundaries of the FE domain: all components of displacements were assumed to be zero along the bottom (horizontal) surface and along the outer, curved (vertical) surface of the soil domain; on the (vertical) boundary surface created by the plane of symmetry, the displacement perpendicular to the boundary was assumed to be zero. A perfect contact (with no slippage or separation) between the pile and the surrounding soil was assumed. The radial distances of the outer curved (vertical) boundary of the soil domain from the pile axis were taken as 20 m and 25 m for the 15 m and 40 m piles respectively; the corresponding vertical distances from the pile base to the bottom (horizontal) boundary of the soil domain were 5 m and 20 m. Twenty-noded brick elements were used to represent both the pile and the soil for both the problems. The element size in the pile and at the pile/soil interface was approximately 0·1 m for both the examples, and was increased gradually with increasing radial distance from the pile axis to 2·0 m (for the 15 m pile) and 3·8 m (for the 40 m pile) at the outer curved boundary of the soil domain. The number of degrees of freedom used for the 15 m pile was 56 653, and that used for the 40 m pile was 90 564. The optimal domains and meshes described above were obtained by ensuring that there were no boundary effects and by performing convergence checks.

The CPU run times of the 3D FE analyses (run in a 16-core x86 server containing eight 2·6 MHz dual-core Opteron 8218 processors with 32 GB RAM) were 9 min (for the 15 m pile) and 14 min (for the 40 m pile), while the CPU run time for our analysis (performed with a Fortran code run in an Intel Centrino Duo 2·0 GHz processor with 2 GB RAM) was 9·75 s for both the examples. Considering the fact that construction of the geometry (domain) and optimal meshing for a FEA requires considerable time, our analysis is much more efficient than FEA because, in addition to being faster, the input to our analysis (the dimensions and elastic properties of pile, and the thickness and elastic constants of soil layers) is accomplished through a simple text file.

Finally, we consider the field example of a laterally loaded pile load test performed by McClelland & Focht (1958). The length (L_p) and radius (r_p) of the pile are 23 m and 0·305 m, and the pile was embedded in a normally consolidated clay. The pile was acted upon by a lateral force $F_a = 300$ kN and a negative moment $M_a = -265$ kNm at the head. Randolph (1981) back-calculated the pile modulus E_p as $68{\cdot}42 \times 10^6$ kN/m^2 from the reported pile flexural rigidity. Randolph (1981) further suggested, based on back-calculation of test results to match his FEA (coupled with Fourier series), that the soil shear modulus profile for this soil deposit can be represented as $G_s = 0{\cdot}8z \times 10^3$ kN/m^3 with $\nu_s = 0{\cdot}3$. We divided the soil profile into four layers and calculated the shear modulus at the middle of each layer, which were considered the representative values for each layer (Table 2). Using these values of soil modulus, we calculated the pile deflection profile using both our analysis and that based on the assumption of Sun (1994). Fig. 9 shows the pile responses. Also plotted are the measured pile response and that obtained by Randolph (1981). Our analysis produces a pile deflection profile that closely matches the measured profile.

We now investigate how an explicit incorporation of soil layering can be useful in obtaining proper pile response. For that purpose, we studied the response of two piles – a short stubby pile with $L_p = 10$ m, $r_p = 0{\cdot}5$ m and $E_p = 25 \times 10^6$ kN/m^2 and a long slender pile with $L_p = 20$ m, $r_p = 0{\cdot}25$ m and $E_p = 25 \times 10^6$ kN/m^2 – for various soil profiles. Both piles are subjected to a horizontal force $F_a = 1000$ kN, and both are assumed to be free at the head and base.

For the short pile ($L_p = 10$ m), we consider the following cases:

(*a*) a homogeneous soil layer with $G_s = 25$ MPa
(*b*) a two-layer system with $H_1 = 2$ m, $G_{s1} = 25$ MPa and $G_{s2} = 50$ MPa

Table 2. Soil properties at the pile load test site of McClelland & Focht (1958)

Depth: m	Extent of soil layers: m	Shear modulus, G_s: MPa
2·0	0 to −4·0	1·6
6·0	−4·0 to −8·0	4·8
10·0	−8·0 to −12·0	8·0
17·5	−12·0 to great depth	14·0

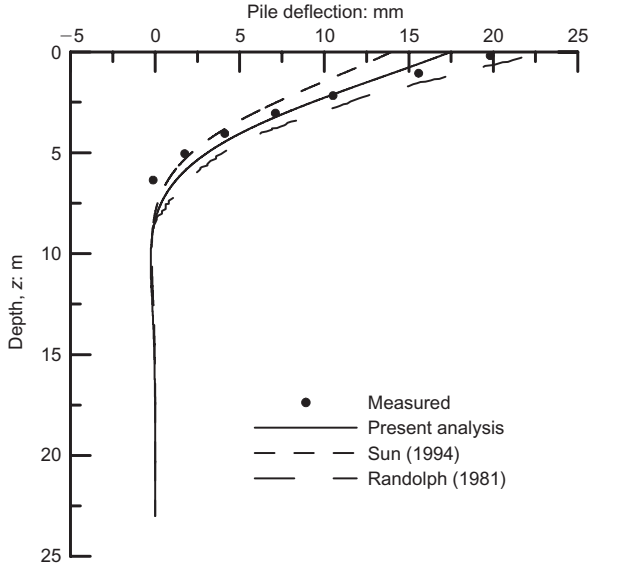

Fig. 9. Deflection profile for the pile load test of McClelland & Focht (1958)

(*c*) a two-layer system with $H_1 = 2$ m, $G_{s1} = 25$ MPa and $G_{s2} = 100$ MPa
(*d*) a two-layer system with $H_1 = 2$ m, $G_{s1} = 50$ MPa and $G_{s2} = 25$ MPa.

The Poisson's ratio was kept constant at 0·25 for all the cases and for all the layers. Figs 10(a), 10(b) and 10(c) show the pile deflection, bending moment and shear force profiles.

Next, we consider the long pile ($L_p = 20$ m) and obtain the pile response for the following cases:

(*a*) a homogeneous soil layer with $G_s = 10$ MPa
(*b*) a four-layer system with $H_1 = 1$ m, $H_2 = 3$ m, $H_3 = 5$ m, $G_{s1} = 10$ MPa, $G_{s2} = 20$ MPa, $G_{s3} = 40$ MPa and $G_{s4} = 80$ MPa
(*c*) a four-layer system with $H_1 = 1$ m, $H_2 = 3$ m, $H_3 = 5$ m, $G_{s1} = 10$ MPa, $G_{s2} = 40$ MPa, $G_{s3} = 40$ MPa and $G_{s4} = 80$ MPa

The Poisson's ratio was again assumed to be 0·25 for all the cases and for all the layers. Figs 11(a) and 11(b) show the pile deflection and bending moment profiles for the above cases respectively.

The effect of soil layering on lateral pile response is evident from Figs 10 and 11. The modulus and thickness of different soil layers (particularly those near the pile head) have a definite effect on lateral pile response. The examples show that proper characterisation of soil deposits and explicit accounting for the different layers are necessary for accurate prediction of pile response and optimal design of laterally loaded piles. Using our analysis, the three-dimensional interaction between pile and soil can be explicitly accounted for with full consideration of soil layering. The assumptions made in the estimation of soil displacements (that the displacements can be represented as products of separable variables, and that the vertical displacement is zero), albeit reasonable, do not strictly represent the exact displacement field for a pile in an ideal elastic soil: consequently, the pile response obtained from this analysis will deviate, even if slightly, from the actual pile response in elastic soil. Notwithstanding the limitations of these assumptions, pile response comparable with those obtained from FEA can be produced at much less time and cost.

In addition to pile deflection, the analysis produces the soil displacement field surrounding a pile (using equation (2)). Thus, if additional piles are present in the neighbourhood of a loaded pile, the effect of the loaded pile on the neighbouring piles can be determined by modifying the analysis. Such an analysis can be further extended to develop a method of analysis of pile groups.

The analysis described in this paper is valid for linear elastic soils. As a result, its use is restricted to those problems for which an equivalent elastic soil modulus can be obtained from field sites. Given that the analysis matches carefully performed FEA rather well, it can be used as a benchmark in future studies. Additionally, the analysis serves as the basis for more elaborate analysis that can take into account soil non-linearity, because the degradation of soil stiffness resulting from progressive yield due to loading of the pile can be obtained from the soil strain field surrounding the pile (equation (3)), which is available as a result of this analysis (in general, modulus degradation of soil depends on the strains induced and on the shear strength of soil).

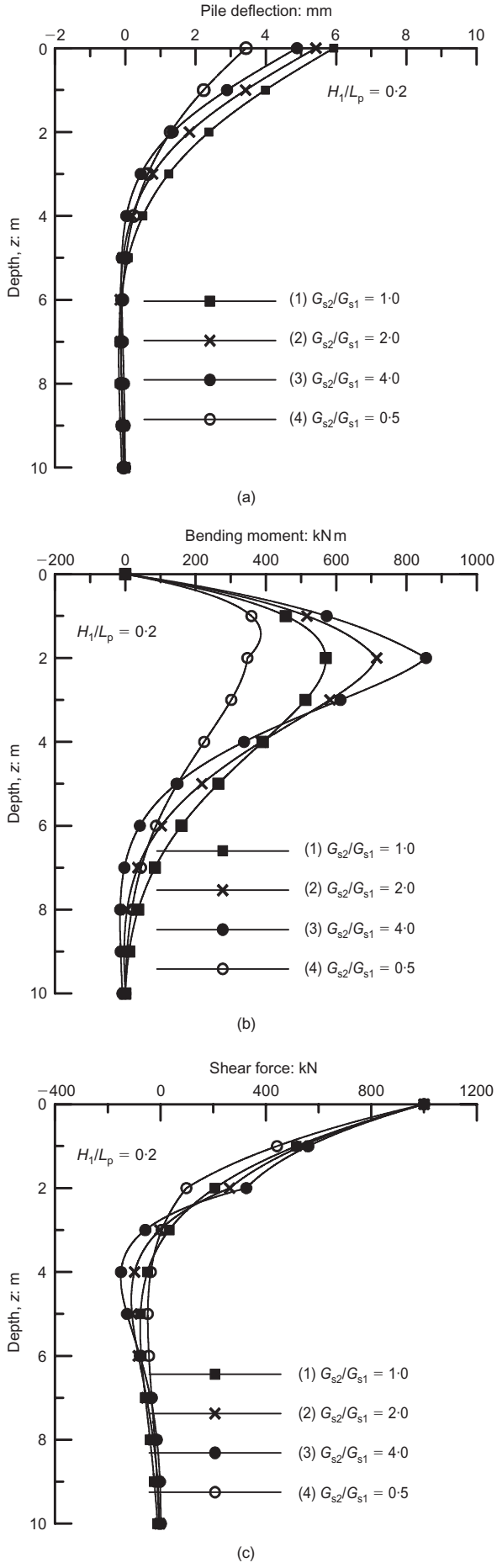

Fig. 10. Effect of layering in a two-layer soil: (a) pile deflection, (b) bending moment and (c) shear force of a 10 m long pile

CONCLUSIONS

An advanced method of analysis for a single, circular pile embedded in a multilayered elastic medium and subjected to a horizontal force and a moment at the head was presented.

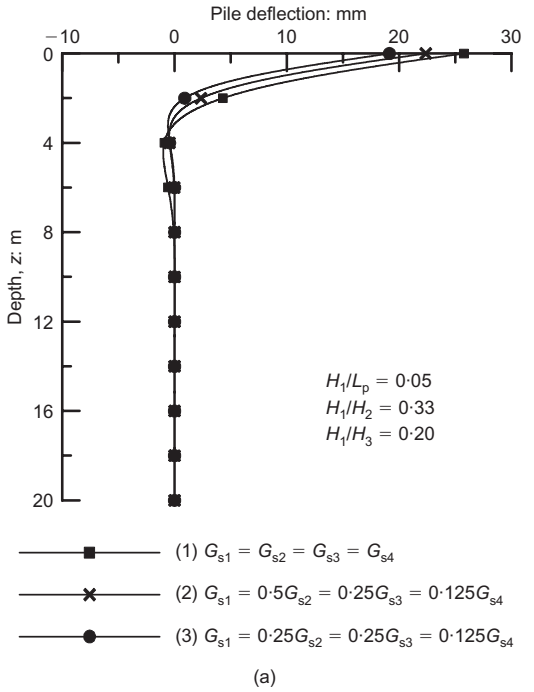

Fig. 11. Effect of layering in a four-layer soil: (a) pile deflection and (b) bending moment of a 20 m long pile

The differential equations governing pile deflection and soil displacements were derived using energy principles. The equation of pile deflection was solved analytically, and the one-dimensional FD method was used to solve the soil displacement equations. The solution is fast, and produces results comparable with 3D FEA. Using this method, pile deflection, slope of the deflection curve, bending moment and shear force for the entire length of the pile can be obtained if the following are known: the pile radius and length, the thicknesses of the soil layers, the Young's modulus of the pile material, the elastic constants of the soil in the various layers, and the magnitudes of the applied force and moment.

The solution depends on a set of parameters γ_1 to γ_6 that determine the rate at which the displacements in the soil medium decay with increasing radial distance from the pile axis. These parameters are not known a priori and must be determined iteratively. Hence an iterative scheme was developed and coded to obtain solutions for a variety of boundary conditions and soil profiles. Notwithstanding the iterations on the γs, the solutions are obtained in seconds.

Illustrations of use of the analysis for layered soils show that soil layering has a definite impact on pile response. Hence proper site characterisation and explicit accounting for the different layers are necessary to predict lateral pile response accurately. The present analysis has the capability to produce pile response with full consideration of soil layering. The analysis can be further extended to account for soil non-linearity, and to analyse pile groups.

ACKNOWLEDGEMENTS

This material is based in part upon work supported by the National Science Foundation under Grant No. 0556347. Tanusree Chakraborty assisted in the finite element analyses, for which we are grateful.

APPENDIX 1

The potential energy density of the soil can be expressed in terms of the displacement functions and elastic constants as

$$\begin{aligned}\frac{1}{2}\sigma_{pq}\varepsilon_{pq} = \frac{1}{2}\Bigg[&(\lambda_s + 2G_s)w^2\left(\frac{d\phi_r}{dr}\right)^2\cos^2\theta \\ &+ 2\lambda_s w^2\frac{d\phi_r}{dr}\frac{(\phi_r-\phi_\theta)}{r}\cos^2\theta \\ &+ (\lambda_s+G_s)w^2\frac{(\phi_r-\phi_\theta)^2}{r^2}\cos^2\theta + G_s w^2\frac{(\phi_r-\phi_\theta)^2}{r^2} \\ &+ G_s w^2\left(\frac{d\phi_\theta}{dr}\right)^2\sin^2\theta + 2G_s w^2\frac{(\phi_r-\phi_\theta)}{r}\frac{d\phi_\theta}{dr}\sin^2\theta \\ &+ G_s\left(\frac{dw}{dz}\right)^2\phi_r^2\cos^2\theta + G_s\left(\frac{dw}{dz}\right)^2\phi_\theta^2\sin^2\theta\Bigg] \end{aligned} \quad (46)$$

Substituting equation (46) in equation (1) and performing integrations with respect to θ produces equation (4). Applying the principle of minimum potential energy to equation (4) results in

$$\begin{aligned}\Bigg\{&\int_0^{L_p} E_p I_p\frac{d^2w}{dz^2}\delta\left(\frac{d^2w}{dz^2}\right)dz. + \pi\int_0^\infty\int_{r_p}^\infty\Bigg[(\lambda_s+2G_s)w\,\delta w\left(\frac{d\phi_r}{dr}\right)^2 \\ &+ 2\lambda_s w\delta w\frac{\phi_r}{r}\frac{d\phi_r}{dr} - 2\lambda_s w\delta w\frac{\phi_\theta}{r}\frac{d\phi_r}{dr} \\ &+ (\lambda_s+3G_s)w\delta w\frac{\phi_r^2}{r^2} + (\lambda_s+3G_s)w\delta w\frac{\phi_\theta^2}{r^2} \\ &- 2(\lambda_s+3G_s)w\delta w\frac{\phi_r\phi_\theta}{r^2} + G_s w\delta w\left(\frac{d\phi_\theta}{dr}\right)^2 + 2G_s w\delta w\frac{\phi_r}{r}\frac{d\phi_\theta}{dr} \\ &- 2G_s w\delta w\frac{\phi_\theta}{r}\frac{d\phi_\theta}{dr} + G_s\frac{dw}{dz}\delta\left(\frac{dw}{dz}\right)\phi_r^2 + G_s\frac{dw}{dz}\delta\left(\frac{dw}{dz}\right)\phi_\theta^2\Bigg]r\,dr\,dz \\ &+ \pi r_p^2\int_{L_p}^\infty G_s\frac{dw}{dz}\delta\left(\frac{dw}{dz}\right)dz - F_a\delta w\Big|_{z=0} + M_a\delta\left(\frac{dw}{dz}\right)\Big|_{z=0}\Bigg\}\end{aligned}$$

$$+\left\{\pi\int_0^{\infty}\int_{r_p}^{\infty}\left[(\lambda_s+2G_s)w^2\left(\frac{d\phi_r}{dr}\right)\delta\left(\frac{d\phi_r}{dr}\right)+\lambda_s w^2\frac{1}{r}\delta\phi_r\frac{d\phi_r}{dr}+\lambda_s w^2\frac{\phi_r}{r}\delta\left(\frac{d\phi_r}{dr}\right)-\lambda_s w^2\frac{\phi_\theta}{r}\delta\left(\frac{d\phi_r}{dr}\right)+(\lambda_s+3G_s)w^2\frac{\phi_r}{r^2}\delta\phi_r\right.\right.$$
$$\left.-(\lambda_s+3G_s)w^2\delta\phi_r\frac{\phi_\theta}{r^2}+G_s w^2\frac{1}{r}\delta\phi_r\frac{d\phi_\theta}{dr}+G_s\left(\frac{dw}{dz}\right)^2\phi_r\delta\phi_r\right]r\,dr\,dz\Bigg\}+\left\{\pi\int_0^{\infty}\int_{r_p}^{\infty}\left[-\lambda_s w^2\frac{1}{r}\delta\phi_\theta\frac{d\phi_r}{dr}+(\lambda_s+3G_s)w^2\frac{\phi_\theta}{r^2}\delta\phi_\theta\right.\right.$$
$$\left.\left.-(\lambda_s+3G_s)w^2\frac{\phi_r}{r^2}\delta\phi_\theta+G_s w^2\frac{d\phi_\theta}{dr}\delta\left(\frac{d\phi_\theta}{dr}\right)+G_s w^2\frac{\phi_r}{r}\delta\left(\frac{d\phi_\theta}{dr}\right)-G_s w^2\frac{1}{r}\delta\phi_\theta\frac{d\phi_\theta}{dr}-G_s w^2\frac{\phi_\theta}{r}\delta\left(\frac{d\phi_\theta}{dr}\right)+G_s\left(\frac{dw}{dz}\right)^2\phi_\theta\delta\phi_\theta\right]r\,dr\,dz\Bigg\}=0 \tag{47}$$

Simplifying further, and considering a layered system (Fig. 1), we get

$$\left\{\int_0^{H_1}\left(E_pI_p\frac{d^4w_1}{dz^4}-2t_1\frac{d^2w_1}{dz^2}+k_1w_1\right)\delta w_1\,dz+\int_{H_1}^{H_2}\left(E_pI_p\frac{d^4w_2}{dz^4}-2t_2\frac{d^2w_2}{dz^2}+k_2w_2\right)\delta w_2\,dz+\ldots.+\int_{H_{n-1}}^{L_p}\left(E_pI_p\frac{d^4w_n}{dz^4}-2t_n\frac{d^2w_n}{dz^2}+k_nw_n\right)\delta w_n\,dz\right.$$
$$+\int_{L_p}^{\infty}\left(-2t_{n+1}\frac{d^2w_{n+1}}{dz^2}+k_nw_{n+1}\right)\delta w_{n+1}\,dz+\left(E_pI_p\frac{d^3w_1}{dz^3}-2t_1\frac{dw_1}{dz}-F_a\right)\delta w_1\Big|_{z=0}-\left(E_pI_p\frac{d^2w_1}{dz^2}-M_a\right)\delta\left(\frac{dw_1}{dz}\right)\Big|_{z=0}$$
$$+\left[-\left(E_pI_p\frac{d^3w_1}{dz^3}-2t_1\frac{dw_1}{dz}\right)\delta w_1\Big|_{z=H_1}+\left(E_pI_p\frac{d^3w_2}{dz^3}-2t_2\frac{dw_2}{dz}\right)\delta w_2\Big|_{z=H_1}\right]+\left[E_pI_p\frac{d^2w_1}{dz^2}\delta\left(\frac{dw_1}{dz}\right)\Big|_{z=H_1}-E_pI_p\frac{d^2w_2}{dz^2}\delta\left(\frac{dw_2}{dz}\right)\Big|_{z=H_1}\right]$$
$$+\ldots.+\left[-\left(E_pI_p\frac{d^3w_n}{dz^3}-2t_n\frac{dw_n}{dz}\right)\delta w_n\Big|_{z=L_p}-2t_{n+1}\frac{dw_{n+1}}{dz}\delta w_{n+1}\Big|_{z=L_p}\right]+E_pI_p\frac{d^2w_n}{dz^2}\delta\left(\frac{dw_n}{dz}\right)\Big|_{z=L_p}+2t_{n+1}\frac{dw_{n+1}}{dz}\delta w_{n+1}\Big|_{z=\infty}\Bigg\}$$
$$+\left\{\int_{r_p}^{\infty}\left[-m_{s1}\left(r\frac{d^2\phi_r}{dr^2}+\frac{d\phi_r}{dr}\right)+(m_{s3}+m_{s2})\frac{d\phi_\theta}{dr}+m_{s4}\frac{\phi_r}{r}-m_{s4}\frac{\phi_\theta}{r}+n_sr\phi_r\right]\delta\phi_r\,dr+m_{s1}r\frac{d\phi_r}{dr}\delta\phi_r\Big|_{r_p}^{\infty}+m_{s3}\phi_r\delta\phi_r\Big|_{r_p}^{\infty}-m_{s3}\phi_\theta\delta\phi_r\Big|_{r_p}^{\infty}\right\}$$
$$+\left\{\int_{r_p}^{\infty}\left[-m_{s2}\left(r\frac{d^2\phi_\theta}{dr^2}+\frac{d\phi_\theta}{dr}\right)-(m_{s2}+m_{s3})\frac{d\phi_r}{dr}+m_{s4}\frac{\phi_\theta}{r}-m_{s4}\frac{\phi_r}{r}+n_sr\phi_\theta\right]\delta\phi_\theta\,dr+m_{s2}r\frac{d\phi_\theta}{dr}\delta\phi_\theta\Big|_{r_p}^{\infty}+m_{s2}\phi_r\delta\phi_\theta\Big|_{r_p}^{\infty}-m_{s2}\phi_\theta\delta\phi_\theta\Big|_{r_p}^{\infty}\right\}=0 \tag{48}$$

APPENDIX 2

The expanded form of the matrix $[\Theta]$ in equation (31) is given by

$$[\Theta]_{4n\times4n}=\begin{bmatrix}[\Theta]^{(\text{Head})}_{\tilde z=0} & [0]_{2\times4} & \cdots & & \cdots & [0]_{2\times4}\\ [\Theta]^{(1)}_{\tilde z=\tilde H_1} & -[\Theta]^{(2)}_{\tilde z=\tilde H_1} & [0]_{4\times4} & \cdots & \cdots & [0]_{4\times4}\\ [0]_{4\times4} & [\Theta]^{(2)}_{\tilde z=\tilde H_2} & -[\Theta]^{(3)}_{\tilde z=\tilde H_2} & [0]_{4\times4} & \cdots & [0]_{4\times4}\\ \vdots & [0]_{4\times4} & \ddots & \ddots & \ddots & \vdots\\ \vdots & \vdots & \ddots & \ddots & \ddots & [0]_{4\times4}\\ [0]_{4\times4} & [0]_{4\times4} & \cdots & [0]_{4\times4} & [\Theta]^{(n-1)}_{\tilde z=\tilde H_{n-1}} & -[\Theta]^{(n)}_{\tilde z=\tilde H_{n-1}}\\ [0]_{2\times4} & [0]_{2\times4} & \cdots & \cdots & [0]_{2\times4} & [\Theta]^{(\text{Base})}_{\tilde z=1}\end{bmatrix} \tag{49}$$

where $[\Theta]^{(i)}_{\tilde z=\tilde H_l}(i=1,2,\ldots n)$ is a 4×4 matrix valid for the ith soil layer. It contains the parameter $\tilde t_i$, the functions Φ_1, Φ_2, Φ_3, Φ_4 and their derivatives (Table 1) calculated at the layer interface $\tilde z=\tilde H_l$ ($l=i-1$ or $l=i$). In its expanded form, $[\Theta]^{(i)}_{\tilde z=\tilde H_l}$ can be expressed as

$$[\Theta]^{(i)}_{\tilde z=\tilde H_l}=\begin{bmatrix}\Phi_1 & \Phi_2 & \Phi_3 & \Phi_4\\ \Phi_1' & \Phi_2' & \Phi_3' & \Phi_4'\\ \Phi_1'' & \Phi_2'' & \Phi_3'' & \Phi_4''\\ \Phi_1-2\tilde t_i\Phi_1''' & \Phi_1-2\tilde t_i\Phi_2''' & \Phi_1-2\tilde t_i\Phi_3''' & \Phi_1-2\tilde t_i\Phi_4'''\end{bmatrix}_{\tilde z=\tilde H_l} \tag{50}$$

The matrix $[\Theta]^{(\text{Head})}_{\tilde z=0}$ has a dimension of 2×4 and is expressed in its expanded form as:

$$[\Theta]^{(\text{Head})}_{\tilde z=0}=\begin{cases}\begin{bmatrix}\Phi_1-2\tilde t_1\Phi_1''' & \Phi_2-2\tilde t_1\Phi_2''' & \Phi_3-2\tilde t_1\Phi_3''' & \Phi_4-2\tilde t_1\Phi_4'''\\ \Phi_1' & \Phi_2' & \Phi_3' & \Phi_4'\end{bmatrix}_{\tilde z=0}; & \text{fixed-head condition}\\ \begin{bmatrix}\Phi_1-2\tilde t_1\Phi_1''' & \Phi_2-2\tilde t_1\Phi_2''' & \Phi_3-2\tilde t_1\Phi_3''' & \Phi_4-2\tilde t_1\Phi_4'''\\ \Phi_1'' & \Phi_2'' & \Phi_3'' & \Phi_4''\end{bmatrix}_{\tilde z=0}; & \text{free-head condition}\end{cases} \tag{51}$$

in which the functions Φ_1, Φ_2, Φ_3, Φ_4 and their derivatives are calculated at $\tilde z=0$ (pile head). The 2×4 matrix $[\Theta]^{(\text{Base})}_{\tilde z=1}$ is given by

$$[\Theta]^{(\text{Base})}_{\tilde z=1}=\begin{cases}\begin{bmatrix}\Phi_1 & \Phi_2 & \Phi_3 & \Phi_4\\ \Phi_1' & \Phi_2' & \Phi_3' & \Phi_4'\end{bmatrix}_{\tilde z=1}; & \text{fixed-base condition}\\ \begin{bmatrix}\Phi_1'''-2\tilde t_n\Phi_1'-\sqrt{2\tilde k_n\tilde t_{n+1}}\Phi_1 & \Phi_2'''-2\tilde t_n\Phi_2'-\sqrt{2\tilde k_n\tilde t_{n+1}}\Phi_2\\ \Phi_1'' & \Phi_2''\\ \Phi_3'''-2\tilde t_n\Phi_3'-\sqrt{2\tilde k_n\tilde t_{n+1}}\Phi_3 & \Phi_4'''-2\tilde t_n\Phi_4'-\sqrt{2\tilde k_n\tilde t_{n+1}}\Phi_4\\ \Phi_3'' & \Phi_4''\end{bmatrix}_{\tilde z=1}; & \text{free-base condition}\end{cases} \tag{52}$$

in which the functions Φ_1, Φ_2, Φ_3, Φ_4 and their derivatives are calculated at $\tilde z=1$ (pile base). The matrices $[0]_{2\times4}$ and $[0]_{4\times4}$ have respectively two rows and four columns and four rows and four columns, and contain '0' as all the elements.

The vector [C] (with a dimension of $4n$) in equation (31) is given by:

$$[\mathrm{C}] = \left[C_1^{(1)} \quad C_2^{(1)} \quad C_3^{(1)} \quad C_4^{(1)} \quad C_1^{(2)} \quad C_2^{(2)} \quad C_3^{(2)} \quad C_4^{(2)} \quad \cdots \quad \cdots \quad C_1^{(n)} \quad C_2^{(n)} \quad C_3^{(n)} \quad C_4^{(n)} \right]^{\mathrm{T}} \tag{53}$$

The superscript T implies the transpose of a matrix.

The right-hand side vector of equation (31) is given by

$$[\mathrm{F}]_{4n\times 1} = \left[\tilde{F}_{\mathrm{a}} \quad \mathrm{F}_2 \quad 0 \quad \cdots \quad \cdots \quad 0 \right]^{\mathrm{T}} \tag{54}$$

with $F_2 = 0$ for the fixed-head condition and $\mathrm{F}_2 = \tilde{M}_{\mathrm{a}}$ for the free-head condition.

REFERENCES

Anderson, J. B., Townsend, F. C. & Grajales, B. (2003). Case history evaluation of laterally loaded piles. *J. Geotech. Geoenviron. Engng ASCE* **129**, No. 3, 187–196.

Ashour, M. & Norris, G. (2000). Modeling lateral soil–pile response based on soil–pile interaction. *J. Geotech. Geoenviron. Engng ASCE* **126**, No. 5, 420–428.

Banerjee, P. K. & Davies, T. G. (1978). The behaviour of axially and laterally loaded single piles embedded in nonhomogeneous soils. *Géotechnique* **28**, No. 3, 309–326.

Bransby, M. F. (1999). Selection of *p–y* curves for the design of single laterally loaded piles. *Int. J. Numer. Anal. Methods Geomech*. **23**, No. 15, 1909–1926.

Briaud, J.-L. (1997). Sallop: simple approach for lateral loads on piles. *J. Geotech. Geoenviron. Engng ASCE* **123**, No. 10, 958–964.

Briaud, J.-L., Smith, T. & Meyer, B. (1984). Laterally loaded piles and the pressuremeter: comparison of existing methods. In *Laterally loaded deep foundations* (eds J. A. Langer, E. T. Mosley and C. C. Thompson), ASTM STP 835, pp. 97–111. Philadelphia, PA: ASTM.

Brown, D. A., Shie, C. & Kumar, M. (1989). *P–y* curves for laterally loaded piles derived from three-dimensional finite element model. *Proc. 3rd Int. Symp. on Numerical Models in Geomechanics (NUMOG III), Niagara Falls*, 683–690.

Brown, D. A., Hidden, S. A. & Zhang, S. (1994). Determination of *p–y* curves using inclinometer data. *Geotech. Test. J.* **17**, No. 2, 150–158.

Budhu, M. & Davies, T. G. (1988). Analysis of laterally loaded piles in soft clays. *J. Geotech. Engng Div. ASCE* **114**, No. 1, 21–39.

Cox, W. R., Reese, L. C. & Grubbs, B. R. (1974). Field testing of laterally loaded piles in sand. *Proc. 6th Offshore Technol. Conf., Houston, TX* **2**, 459–472.

Gabr, M. A., Lunne, T. & Powell, J. J. (1994). *P–y* analysis of laterally loaded piles in clay using DMT. *J. Geotech. Engng ASCE* **120**, No. 5, 816–837.

Guo, W. D. & Lee, F. H. (2001). Load transfer approach for laterally loaded piles. *Int. J. Numer. Anal. Methods Geomech.* **25**, No. 11, 1101–1129.

Kim, B. T., Kim, N.-K., Lee, W. J. & Kim, Y. S. (2004). Experimental load-transfer curves of laterally loaded piles in Nak-Dong river sand. *J. Geotech. Geoenviron. Engng ASCE* **130**, No. 4, 416–425.

Klar, A. & Frydman, S. (2002). Three-dimensional analysis of lateral pile response using two-dimensional explicit numerical scheme. *J. Geotech. Geoenviron. Engng ASCE* **128**, No. 9, 775–784.

Matlock, H. (1970). Correlations for design of laterally loaded piles in soft clay. *Proc. 2nd Offshore Technol. Conf., Houston, TX* **1**, 577–594.

McClelland, B. & Focht, J. A. Jr (1958). Soil modulus for laterally loaded piles. *Trans. ASCE* **123**, 1049–1063.

Mindlin, R. D. (1936). Force at a point in the interior of a semi-infinite solid. *Physics* **7**, May, 195–202.

Ng, C. W. W. & Zhang, L. M. (2001). Three-dimensional analysis of performance of laterally loaded sleeved piles in sloping ground. *J. Geotech. Geoenviron. Engng ASCE* **127**, No. 6, 499–509.

Pise, P. J. (1982). Laterally loaded piles in a two-layer soil system. *J. Geotech. Engng Div. ASCE* **108**, No. GT9, 1177–1181.

Poulos, H. G. (1971a). Behavior of laterally loaded piles: I – single piles. *J. Soil Mech. Found. Div. ASCE* **97**, No. SM5, 711–731.

Poulos, H. G. (1971b). Behavior of laterally loaded piles: III – socketed piles. *J. Soil Mech. Found. Div. ASCE* **98**, No. SM4, 341–360.

Poulos, H. G. (1973). Load–deflection prediction for laterally loaded piles. *Aust. Geomech. J.* **G3**, No. 1, 1–8.

Randolph, M. F. (1981). The response of flexible piles to lateral loading. *Géotechnique* **31**, No. 2, 247–259.

Reese, L. C. & Cox, W. R. (1969). Soil behavior from analysis of tests of uninstrumented piles under lateral loading. In *Performance of deep foundations*, ASTM STP 444, pp. 160–176. Philadelphia, PA: ASTM.

Reese, L. C. & Van Impe, W. F. (2001). *Single piles and pile groups under lateral loading*. Rotterdam: A. A. Balkema.

Reese, L. C., Cox, W. R. & Koop, F. D. (1974). Analysis of laterally loaded piles in sand. *Proc. 6th Offshore Technol. Conf., Houston, TX* **2**, 473–483.

Reese, L. C., Cox, W. R. & Koop, F. D. (1975). Field testing and analysis of laterally loaded piles in stiff clay. *Proc. 7th Offshore Technol. Conf., Houston, TX* **2**, 671–690.

Sun, K. (1994). Laterally loaded piles in elastic media. *J. Geotech. Engng ASCE* **120**, No. 8, 1324–1344.

Trochanis, A. M., Bielak, J. & Christiano, P. (1991). Three-dimensional nonlinear study of piles. *J. Geotech. Engng ASCE* **117**, No. 3, 429–447.

Verruijt, A. & Kooijman, A. P. (1989). Laterally loaded piles in a layered elastic medium. *Géotechnique* **39**, No. 1, 39–46.

Vlasov, V. Z. & Leont'ev, N. N. (1966). *Beams, plates and shells on elastic foundations*. Jerusalem: Israel Program for Scientific Translations.

Winkler, E. (1867). *Die Lehre von der Elasticitaet und Festigkeit*. Prague: Dominicus.

Wu, D., Broms, B. B. & Choa, V. (1998). Design of laterally loaded piles in cohesive soils using *p–y* curves. *Soils Found.* **38**, No. 2, 17–26.

Yan, L. & Byrne, P. M. (1992). Lateral pile response to monotonic pile head loading. *Can. Geotech. J.* **29**, 955–970.

Zhang, L., Ernst, H. & Einstein, H. H. (2000). Nonlinear analysis of laterally loaded rock-socketed shafts. *J. Geotech. Geoenviron. Engng ASCE* **126**, No. 11, 955–968.